Scattering of elastic waves by a sphere with orthorhombic anisotropy and application to polycrystalline material characterization

Citation for the original published paper (version of record):
Jafarzadeh, A., Folkow, P., Boström, A. (2024). Scattering of elastic waves by a sphere with orthorhombic anisotropy and application to polycrystalline material characterization. Ultrasonics, 138.
http://dx.doi.org/10.1016/j.ultras.2023.107199

Ultrasonics 138 (2024) 107199

Contents lists available at ScienceDirect

Ultrasonics

journal homepage: www.elsevier.com/locate/ultras

Scattering of elastic waves by a sphere with orthorhombic anisotropy and application to polycrystalline material characterization

Ata Jafarzadeh *, Peter D. Folkow, Anders Boström

Chalmers University of Technology, Department of Mechanics and Maritime Sciences, Horsalsvagen 7, SE-412 96, Gothenburg, Sweden

ARTICLE INFO

Dataset link: Supplementary Documents (Original data)

Keywords:
Elastic wave scattering
Orthorhombic anisotropy
Spherical inclusion
Polycrystal
Effective wave number

ABSTRACT

Scattering of elastic waves by an anisotropic sphere with orthorhombic symmetry inside an isotropic medium is studied and applied to characterization of polycrystalline materials with anisotropic grains. For a single sphere the waves in the isotropic surrounding are expanded in the spherical vector wave functions. Inside the sphere, the elastodynamic equations are first transformed to spherical coordinates and the displacement field is expanded in terms of the vector spherical harmonics in the angular directions and power series in the radial direction. The governing equations inside the sphere give recursion relations among the expansion coefficients in the power series. The boundary conditions on the sphere then determine the relation among the scattered wave expansion coefficients and those of the incident wave, expressed as the transition (**T**) matrix. For low frequencies the elements of the **T** matrix are obtained in explicit form. According to the theory of Foldy the **T** matrix elements of a single sphere are used to study attenuation and phase velocity of polycrystalline materials, explicitly for low frequencies. Comparisons of the present method with previously published results and recent FEM results show a good correspondence for low frequencies. The present approach shows a better agreement with FEM for strongly anisotropic materials in comparison with other published methods.

1. Introduction

The study of wave propagation and scattering in inhomogeneous media have received extensive attention due to the need for the characterization of such media. The scattering of elastic waves by anisotropic grains in polycrystals is a classical problem that has important practical applications in various fields, such as seismology and non-destructive evaluation. Polycrystalline materials consist of numerous small crystals, also known as grains, which are typically anisotropic. Although the elastic constants are identical for all grains within a single phase polycrystalline material, the orientation is different for each grain. If the grains are randomly oriented and equiaxed, the overall properties of the material become isotropic. However, the presence of these grains leads to wave scattering and hence attenuation. To estimate the attenuation and effective phase velocity in polycrystals, different models such as individual particles, a regular array of particles, or a stochastic process can be used [1]. In their work Stanke and Kino [1] address different aspects of each geometrical model and utilize a stochastic process to estimate the attenuation and phase velocity of polycrystalline materials with equiaxed anisotropic grains of cubic symmetry. In this approach, the micro-inhomogeneous elastic polycrystal is commonly simplified by replacing it with a mean isotropic medium, usually through a Voigt average of the properties of the crystal, and a continuous random fluctuation to account for the inhomogeneity of the medium. This approximation is referred to as the second order approximation (SOA), because it assumes that the second order degree of inhomogeneity is small. This methodology is further developed to compare attenuation in two and three dimensional polycrystals [2] and investigates the effect of various geometrical properties [3–7] as well as the anisotropy symmetries [6,8–10] of the crystals. These advancements in the SOA method have recently been employed for non-destructive ultrasonic characterization of polycrystals [11,12]. Another method is the self-consistent approach (SCA), proposed by Kube and Turner [13], where the mean elastic medium is determined through a self-consistent average instead of the Voigt average. The experimental wave velocity data evaluated against the SOA and SCA reveal a better agreement when the Voigt reference is used in second order models [14]. A more extensive evaluation of the SOA method and its development are presented in the literature [6,15].

Development of the finite element method for investigation of phase velocity and attenuation in polycrystalline materials [15–19] suggests that the SOA models are not accurate when the grains are highly anisotropic and the degree of inhomogeneity increases, particularly in the low

* Corresponding author.
E-mail address: jata@chalmers.se (A. Jafarzadeh).

https://doi.org/10.1016/j.ultras.2023.107199
Received 4 May 2023; Received in revised form 6 November 2023; Accepted 8 November 2023
Available online 20 November 2023

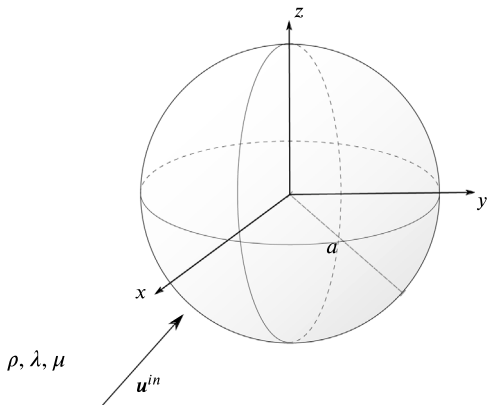

Fig. 1. The orthorhombic sphere with radius a and the incident wave $\boldsymbol{u}^{in}$.

frequency limit [15,19,20]. To address this issue, Huang et al. [15,19] develop approximation methods that consider the quadratic order of the degree of inhomogeneity in the SOA method. While these approximation methods are effective in estimating phase velocities accurately, there is still room for improvement in the estimation of attenuation [15].

Polycrystals can also be regarded as a special case of a medium with a distribution of inclusions. The attenuation and effective phase velocity in polycrystals can then be estimated by examining how waves scatter from individual grains. Foldy [21] develops a methodology to estimate the effective wave number of a medium with a distribution of inclusions (regarded as point scatterers) for scalar waves. This approach is further developed regarding correlations among scatterers positions, [22] elastic waves scattering and volume scatterers [23,24]. Kanaun and Levin [25] referred to this neglection as the one particle solution. Based on the definition of the surrounding medium of the particle and the field acting on it, they provided a comprehensive overview of different approaches, including Foldy theory, for studying the dynamic response of inhomogeneous mediums with bounded inhomogeneities. In the case of polycrystalline materials, where grains possess anisotropic properties, it is necessary to consider the one particle solution of an anisotropic grain. For this purpose, Kanaun and Levin [25] assumed that the surrounding medium of the single particle is equivalent to the effective medium of the polycrystal. By using an integral representation method, the solution of the one particle problem is related to the Green function of the surrounding medium and the average of the elasticity tensor of the anisotropic particle over all orientations.

Boström [26] further investigated the one particle problem with orthorhombic symmetry of a spherical particle using series expansions of the fields inside and outside of the particle and evaluated effective wave numbers of polycrystals with anisotropic grains in 2D [27]. Similarly, Jafarzadeh et al. [28,29] extend this study to 3D problems by calculating the transition (**T**) matrix of a single transversely anisotropic or cubic sphere, respectively, and estimate wave numbers in polycrystals with these crystal symmetries. Although these studies are limited to low and intermediate frequencies, they show good correspondence with FEM in estimating wave numbers in polycrystals with strongly anisotropic crystals.

The aim of this work is to characterize polycrystalline materials by finding the **T** matrix elements for a spherical obstacle with orthorhombic symmetry in an isotropic surrounding. The same approach as for a spherical obstacle with transverse isotropy [28] or cubic anisotropy [29] is taken. Expressing the constitutive equations for a material with orthorhombic symmetry in spherical coordinates reveals the complexity of the governing equations, involving explicit trigonometric functions in both the polar and azimuthal coordinates. By using expansions in vector spherical harmonics and power series in the angular and radial coordinates, respectively, the equations of motion result in recursion relations for the coefficients in the power series. The boundary conditions are applied and the **T** matrix elements for a single spherical obstacle are derived. These elements are employed along with Foldy theory to calculate the attenuation and phase velocity of polycrystalline materials explicitly for low frequencies. In addition to the explicit expression, a numerical calculation is performed to evaluate the attenuation and phase velocities for both low and intermediate frequencies. Overall, the paper contributes to a better understanding of wave propagation in polycrystalline materials with orthorhombic anisotropy.

2. Statement of the problem

Consider the scattering by a single spherical inclusion with radius a and orthorhombic material properties inside an isotropic full space, see Fig. 1. A known wave is incident on the inclusion and is assumed to be monochromatic with a fixed angular frequency ω (the time factor $\exp(-i\omega t)$ is suppressed). In this section wave propagation in the isotropic surrounding with density ρ and Lamé parameters λ and μ is reviewed, and in the following section the material properties and waves inside the anisotropic sphere are studied.

The wave numbers in the isotropic medium are $k_p^2 = \rho\omega^2/(\lambda + 2\mu)$ and $k_s^2 = \rho\omega^2/\mu$ for longitudinal and transverse waves, respectively. For the spherical inclusion it is of course natural to use spherical coordinates (r, θ, φ). It is then convenient to use spherical vector wave functions $\boldsymbol{\psi}_{\tau\sigma ml}$ to express field quantities in the isotropic medium. These functions are defined as [30]

$$\boldsymbol{\psi}^0_{1\sigma ml}(r,\theta,\varphi) = \frac{1}{\sqrt{l(l+1)}} \nabla \times \left(j_l(k_s r) Y_{\sigma ml}(\theta,\varphi) \right), \tag{1}$$

$$\boldsymbol{\psi}^0_{2\sigma ml}(r,\theta,\varphi) = \frac{1}{\sqrt{l(l+1)}} \frac{1}{k_s} \nabla \times \nabla \times \left(j_l(k_s r) Y_{\sigma ml}(\theta,\varphi) \right), \tag{2}$$

$$\boldsymbol{\psi}^0_{3\sigma ml}(r,\theta,\varphi) = \left(\frac{k_p}{k_s} \right)^{3/2} \frac{1}{k_p} \nabla \left(j_l(k_p r) Y_{\sigma ml}(\theta,\varphi) \right). \tag{3}$$

The spherical vector wave functions are constructed from the derivatives of the spherical scalar wave functions, which are a product of a spherical Bessel function in the radial coordinate and a spherical harmonic in the polar and azimuthal coordinates. The spherical harmonics are defined as

$$Y_{\sigma ml}(\theta,\varphi)=\sqrt{\frac{\epsilon_m(2l+1)(l-m)!}{4\pi(l+m)!}}P_l^m(\cos\theta)\begin{Bmatrix}\cos m\varphi\\ \sin m\varphi\end{Bmatrix}, \tag{4}$$

where, $P_l^m(\cos\theta)$ is an associated Legendre function of order m and degree l. The Neumann factor is ϵ_m with $\epsilon_0=1$ and $\epsilon_m=2$ for $m=1,2,\ldots$. Also, $\sigma=e$ is for the upper row which is even with respect to φ and $\sigma=o$ is for the lower row which is odd with respect to φ. It is then convenient to define vector spherical harmonics from the derivative of the spherical harmonics as

$$\begin{aligned}
\boldsymbol{A}_{1\sigma ml}(\theta,\varphi)&=\frac{1}{\sqrt{l(l+1)}}\nabla\times(\boldsymbol{r}Y_{\sigma ml}(\theta,\varphi))\\
&=\frac{1}{\sqrt{l(l+1)}}\left(\boldsymbol{e}_\theta\frac{1}{\sin\theta}\frac{\partial}{\partial\varphi}Y_{\sigma ml}(\theta,\varphi)-\boldsymbol{e}_\varphi\frac{\partial}{\partial\theta}Y_{\sigma ml}(\theta,\varphi)\right),\\
\boldsymbol{A}_{2\sigma ml}(\theta,\varphi)&=\frac{1}{\sqrt{l(l+1)}}r\nabla Y_{\sigma ml}(\theta,\varphi)\\
&=\frac{1}{\sqrt{l(l+1)}}\left(\boldsymbol{e}_\theta\frac{\partial}{\partial\theta}Y_{\sigma ml}(\theta,\varphi)+\boldsymbol{e}_\varphi\frac{1}{\sin\theta}\frac{\partial}{\partial\varphi}Y_{\sigma ml}(\theta,\varphi)\right),\\
\boldsymbol{A}_{3\sigma ml}(\theta,\varphi)&=\boldsymbol{e}_rY_{\sigma ml}(\theta,\varphi).
\end{aligned} \tag{5}$$

The vector spherical harmonics constitute a complete orthonormal vector basis system on the unit sphere for vector valued functions. The spherical vector wave functions can then be expressed as

$$\boldsymbol{\psi}^0_{1\sigma ml}(r,\theta,\varphi)=j_l(k_sr)\boldsymbol{A}_{1\sigma ml}(\theta,\varphi), \tag{6}$$

$$\boldsymbol{\psi}^0_{2\sigma ml}(r,\theta,\varphi)=\left(j_l'(k_sr)+\frac{j_l(k_sr)}{k_sr}\right)\boldsymbol{A}_{2\sigma ml}(\theta,\varphi)+\sqrt{l(l+1)}\,\frac{j_l(k_sr)}{k_sr}\boldsymbol{A}_{3\sigma ml}(\theta,\varphi), \tag{7}$$

$$\boldsymbol{\psi}^0_{3\sigma ml}(r,\theta,\varphi)=\left(\frac{k_p}{k_s}\right)^{3/2}\left(j_l'(k_pr)\boldsymbol{A}_{3\sigma ml}(\theta,\varphi)+\sqrt{l(l+1)}\,\frac{j_l(k_pr)}{k_pr}\boldsymbol{A}_{2\sigma ml}(\theta,\varphi)\right). \tag{8}$$

The first index $\tau=1,2,3$ specifies the type of the partial wave according to SH, SV, and P waves, respectively. The index $\sigma=e$ (even) and o (odd) indicates the parity of the wave with respect to the azimuthal coordinate, and the order is $m=0,1,\ldots$ and the degree is $l=m,m+1,\ldots$ ($l=0$ is only relevant for the P wave functions and is not defined for the others). The upper index "0" denotes the regular wave functions which contain spherical Bessel functions. The corresponding outgoing wave functions are denoted by the upper index "+" and contain spherical Hankel functions of the first kind to fulfill the radiation condition.

In the boundary conditions the radial traction is needed. This traction can be written

$$\boldsymbol{t}^{(r)}=\boldsymbol{e}_r\lambda\nabla\cdot\boldsymbol{u}+\mu\left(2\frac{\partial\boldsymbol{u}}{\partial r}+\boldsymbol{e}_r\times(\nabla\times\boldsymbol{u})\right), \tag{9}$$

The corresponding traction for each of the vector wave functions becomes

$$\boldsymbol{t}^{(r)}\left(\boldsymbol{\psi}^0_{1\sigma ml}(\boldsymbol{r})\right)=\mu r\frac{d}{dr}\left(\frac{j_l\left(k_sr\right)}{r}\right)\boldsymbol{A}_{1\sigma ml}\left(\theta,\varphi\right), \tag{10}$$

$$\begin{aligned}
\boldsymbol{t}^{(r)}\left(\boldsymbol{\psi}^0_{2\sigma ml}(\boldsymbol{r})\right)=\mu\Bigg[&\left(2k_sj_l''\left(k_sr\right)+\frac{2j_l'\left(k_sr\right)}{r}-\frac{2j_l\left(k_sr\right)}{k_sr^2}+k_sj_l\left(k_sr\right)\right)\boldsymbol{A}_{2\sigma ml}\left(\theta,\varphi\right)\\
&+2\sqrt{l\left(l+1\right)}\,\frac{d}{dr}\left(\frac{j_l\left(k_sr\right)}{k_sr}\right)\boldsymbol{A}_{3\sigma ml}\left(\theta,\varphi\right)\Bigg],
\end{aligned} \tag{11}$$

$$\begin{aligned}
\boldsymbol{t}^{(r)}\left(\boldsymbol{\psi}^0_{3\sigma ml}(\boldsymbol{r})\right)=\mu\left(\frac{k_p}{k_s}\right)^{3/2}\Bigg[&\left(2k_pj_l''\left(k_pr\right)+\frac{2k_p^2-k_s^2}{k_p}j_l\left(k_pr\right)\right)\boldsymbol{A}_{3\sigma ml}\left(\theta,\varphi\right)\\
&+2\sqrt{l\left(l+1\right)}\,\frac{d}{dr}\left(\frac{j_l\left(k_pr\right)}{k_pr}\right)\boldsymbol{A}_{2\sigma ml}\left(\theta,\varphi\right)\Bigg],
\end{aligned} \tag{12}$$

The total wave outside the sphere is a sum of the incident and scattered waves $\boldsymbol{u}(\boldsymbol{r})=\boldsymbol{u}^0(\boldsymbol{r})+\boldsymbol{u}^+(\boldsymbol{r})$. Since the source of the incident wave is assumed outside the sphere the incident wave can be expanded in terms of the regular wave functions and as the scattered wave must fulfill the radiation condition it can be expanded in the outgoing wave functions

$$\begin{aligned}
\boldsymbol{u}^0(\boldsymbol{r})&=\sum_{\tau\sigma ml}b_{\tau\sigma ml}\boldsymbol{\psi}^0_{\tau\sigma ml}(\boldsymbol{r}),\\
\boldsymbol{u}^+(\boldsymbol{r})&=\sum_{\tau\sigma ml}h_{\tau\sigma ml}\boldsymbol{\psi}^+_{\tau\sigma ml}(\boldsymbol{r}).
\end{aligned} \tag{13}$$

where the sums run through $\tau=1,2,3$, $\sigma=e,o$, $m=0,1,..$, $l=m,m+1,\ldots$. The expansion coefficients of the incident wave $b_{\tau\sigma ml}$ are in principle known and the ones of the scattered wave $h_{\tau\sigma ml}$ are to be determined. A general way to represent the scattering by an obstacle is to determine the transition matrix (**T** matrix) which gives the linear relation between the expansion coefficients of the incident and scattered waves

$$h_{\tau\sigma ml}=\sum_{\tau'\sigma'm'l'}T_{\tau\sigma ml,\tau'\sigma'm'l'}b_{\tau'\sigma'm'l'}. \tag{14}$$

This completes the necessary information in the surrounding medium to solve the scattering problem. In the following sections the anisotropic sphere is analyzed and the transition matrix is derived.

3. The orthorhombic sphere

In this section the material properties and governing equations of the orthorhombic sphere are described, then the waves are expanded using appropriate series. Starting with the material properties, the sphere has density ρ_1 and material properties of orthorhombic symmetry in Cartesian coordinates. The constitutive relations can be expressed using reduced notation as

$$\begin{Bmatrix}\sigma_{xx}\\ \sigma_{yy}\\ \sigma_{zz}\\ \sigma_{yz}\\ \sigma_{zx}\\ \sigma_{xy}\end{Bmatrix}=\begin{bmatrix}C_{11} & C_{12} & C_{13} & 0 & 0 & 0\\ C_{12} & C_{22} & C_{23} & 0 & 0 & 0\\ C_{13} & C_{23} & C_{33} & 0 & 0 & 0\\ 0 & 0 & 0 & 2C_{44} & 0 & 0\\ 0 & 0 & 0 & 0 & 2C_{55} & 0\\ 0 & 0 & 0 & 0 & 0 & 2C_{66}\end{bmatrix}\begin{Bmatrix}\epsilon_{xx}\\ \epsilon_{yy}\\ \epsilon_{zz}\\ \epsilon_{yz}\\ \epsilon_{zx}\\ \epsilon_{xy}\end{Bmatrix}. \tag{15}$$

where $C_{11}, C_{12}, C_{13}, C_{22}, C_{23}, C_{33}, C_{44}, C_{55}$, and C_{66} are nine independent stiffness constants.

The governing elastodynamic equations are expressed in spherical coordinates

$$\frac{\partial\sigma_{rr}}{\partial r}+\frac{1}{r}\frac{\partial\sigma_{r\theta}}{\partial\theta}+\frac{1}{r\sin\theta}\frac{\partial\sigma_{\varphi r}}{\partial\varphi}+\frac{1}{r}\left(2\sigma_{rr}-\sigma_{\theta\theta}-\sigma_{\varphi r}+\cot\theta\sigma_{r\theta}\right)-\rho_1\frac{\partial^2 u_r}{\partial t^2}=0, \tag{16}$$

$$\frac{\partial\sigma_{r\theta}}{\partial r}+\frac{1}{r}\frac{\partial\sigma_{\theta\theta}}{\partial\theta}+\frac{1}{r\sin\theta}\frac{\partial\sigma_{\theta\varphi}}{\partial\varphi}+\frac{1}{r}\left(\cot\theta\left(\sigma_{\theta\theta}-\sigma_{\varphi\varphi}\right)+3\sigma_{r\theta}\right)-\rho_1\frac{\partial^2 u_\theta}{\partial t^2}=0, \tag{17}$$

$$\frac{\partial\sigma_{\varphi r}}{\partial r}+\frac{1}{r}\frac{\partial\sigma_{\theta\varphi}}{\partial\theta}+\frac{1}{r\sin\theta}\frac{\partial\sigma_{\varphi\varphi}}{\partial\varphi}+\frac{1}{r}\left(3\sigma_{\varphi r}+2\cot\theta\sigma_{\theta\varphi}\right)-\rho_1\frac{\partial^2 u_\varphi}{\partial t^2}=0. \tag{18}$$

For the present problem it is convenient to transform the constitutive relations in Eq. (15) from Cartesian to spherical coordinates (see Jafarzadeh et al. [28]). In spherical coordinates the stress–strain relations for a material with orthorhombic properties become

$$\begin{aligned}\sigma_{rr}=&\left(\alpha_1+2\alpha_2\right)\epsilon_{rr}+\alpha_1\epsilon_{\theta\theta}+\left(\alpha_1-\beta_2+\beta_3\right)\epsilon_{\varphi\varphi}-\left(2\beta_1\epsilon_{rr}+\beta_3\epsilon_{\varphi\varphi}\right)\cos 2\theta+\beta_2\left(\epsilon_{rr}-\epsilon_{\theta\theta}\right)\cos 4\theta\\&+2\beta_1\epsilon_{r\theta}\sin 2\theta-2\beta_2\epsilon_{r\theta}\sin 4\theta+\cos 2\varphi\Big[2\beta_5\left(\epsilon_{rr}+3\epsilon_{\theta\theta}-2\epsilon_{\varphi\varphi}\right)+4\beta_6\left(\epsilon_{rr}-\epsilon_{\theta\theta}\right)+\beta_7\left(3\epsilon_{rr}+\epsilon_{\theta\theta}\right)\\&-4\left(\beta_5\epsilon_{\varphi\varphi}+\beta_7\epsilon_{rr}\right)\cos 2\theta-\left(2\beta_5+4\beta_6-\beta_7\right)\left(\epsilon_{rr}-\epsilon_{\theta\theta}\right)\cos 4\theta+4\beta_7\epsilon_{r\theta}\sin 2\theta\\&+2\left(2\beta_5+4\beta_6-\beta_7\right)\epsilon_{r\theta}\sin 4\theta\Big]+\beta_4\cos 4\varphi\Big[3\epsilon_{rr}+\epsilon_{\theta\theta}-4\epsilon_{\varphi\varphi}+4\left(\epsilon_{\varphi\varphi}-\epsilon_{rr}\right)\cos 2\theta+4\epsilon_{r\theta}\sin 2\theta\\&+\left(\epsilon_{rr}-\epsilon_{\theta\theta}\right)\cos 4\theta-2\epsilon_{r\theta}\sin 4\theta\Big]+\sin 2\varphi\Big[-2\left(2\beta_5+4\beta_6-\beta_7\right)\left(\epsilon_{\theta\varphi}\cos 3\theta+\epsilon_{\varphi r}\sin 3\theta\right)\\&-2\left(6\beta_5-4\beta_6+\beta_7\right)\epsilon_{\theta\varphi}\cos\theta-2\left(2\beta_5+4\beta_6+3\beta_7\right)\epsilon_{\varphi r}\sin\theta\Big]+4\beta_4\sin 4\varphi\Big[\epsilon_{\theta\varphi}(\cos 3\theta-\cos\theta)\\&+\epsilon_{\varphi r}(\sin 3\theta-3\sin\theta)\Big],\end{aligned} \tag{19}$$

$$\begin{aligned}\sigma_{\theta\theta}=&\alpha_1\epsilon_{rr}+\left(\alpha_1+2\alpha_2\right)\epsilon_{\theta\theta}+\left(\alpha_1-\beta_2+\beta_3\right)\epsilon_{\varphi\varphi}+\left(2\beta_1\epsilon_{\theta\theta}+\beta_3\epsilon_{\varphi\varphi}\right)\cos 2\theta+\beta_2\left(\epsilon_{\theta\theta}-\epsilon_{rr}\right)\cos 4\theta\\&+2\beta_1\epsilon_{r\theta}\sin 2\theta+2\beta_2\epsilon_{r\theta}\sin 4\theta+\cos 2\varphi\Big[2\beta_5\left(3\epsilon_{rr}+\epsilon_{\theta\theta}-2\epsilon_{\varphi\varphi}\right)-4\beta_6\left(\epsilon_{rr}-\epsilon_{\theta\theta}\right)+\beta_7\left(\epsilon_{rr}+3\epsilon_{\theta\theta}\right)\\&+4\left(\beta_7\epsilon_{\theta\theta}+\beta_5\epsilon_{\varphi\varphi}\right)\cos 2\theta+\left(2\beta_5+4\beta_6-\beta_7\right)\left(\epsilon_{rr}-\epsilon_{\theta\theta}\right)\cos 4\theta+4\beta_7\epsilon_{r\theta}\sin 2\theta\\&-2\left(2\beta_5+4\beta_6-\beta_7\right)\epsilon_{r\theta}\sin 4\theta\Big]+\beta_4\cos 4\varphi\Big[\epsilon_{rr}+3\epsilon_{\theta\theta}-4\epsilon_{\varphi\varphi}+4\left(\epsilon_{\theta\theta}-\epsilon_{\varphi\varphi}\right)\cos 2\theta+4\epsilon_{r\theta}\sin 2\theta\\&+\left(\epsilon_{\theta\theta}-\epsilon_{rr}\right)\cos 4\theta+2\epsilon_{r\theta}\sin 4\theta\Big]+\sin 2\varphi\Big[2\left(2\beta_5+4\beta_6-\beta_7\right)\left(\epsilon_{\theta\varphi}\cos 3\theta+\epsilon_{\varphi r}\sin 3\theta\right)\\&-2\left(2\beta_5+4\beta_6+3\beta_7\right)\epsilon_{\theta\varphi}\cos\theta-2\left(6\beta_5-4\beta_6+\beta_7\right)\epsilon_{\varphi r}\sin\theta\Big]-4\beta_4\sin 4\varphi\Big[\epsilon_{\theta\varphi}(3\cos\theta+\cos 3\theta)\\&+\epsilon_{\varphi r}(\sin\theta+\sin 3\theta)\Big],\end{aligned} \tag{20}$$

$$\begin{aligned}\sigma_{\varphi\varphi}=&\left(\alpha_1-\beta_2+\beta_3\right)\left(\epsilon_{rr}+\epsilon_{\theta\theta}\right)+\left(\alpha_1+2\alpha_2+2\beta_1+\beta_2\right)\epsilon_{\varphi\varphi}+\beta_3\left(\left(\epsilon_{\theta\theta}-\epsilon_{rr}\right)\cos 2\theta+2\epsilon_{r\theta}\sin 2\theta\right)\\&+\cos 2\varphi\Big[-4\beta_5\left(\epsilon_{rr}+\epsilon_{\theta\theta}\right)-8\beta_7\epsilon_{\varphi\varphi}-4\beta_5\left(\left(\epsilon_{rr}-\epsilon_{\theta\theta}\right)\cos 2\theta-2\epsilon_{r\theta}\sin 2\theta\right)\Big]\\&+4\beta_4\cos 4\varphi\Big[2\epsilon_{\varphi\varphi}-\epsilon_{rr}-\epsilon_{\theta\theta}+\left(\epsilon_{rr}-\epsilon_{\theta\theta}\right)\cos 2\theta-2\epsilon_{r\theta}\sin 2\theta\Big]-8\beta_7\sin 2\varphi\Big[\epsilon_{\theta\varphi}\cos\theta+\epsilon_{\varphi r}\sin\theta\Big]\\&+16\beta_4\sin 4\varphi\Big[\epsilon_{\theta\varphi}\cos\theta+\epsilon_{\varphi r}\sin\theta\Big],\end{aligned} \tag{21}$$

$$\begin{aligned}\sigma_{r\theta}=&2\alpha_2\epsilon_{r\theta}+\left(\beta_3\epsilon_{\varphi\varphi}+\beta_1\left(\epsilon_{rr}+\epsilon_{\theta\theta}\right)\right)\sin 2\theta+\beta_2\left(\left(\epsilon_{\theta\theta}-\epsilon_{rr}\right)\sin 4\theta-2\epsilon_{r\theta}\cos 4\theta\right)\\&+\cos 2\varphi\Big[2\left(-2\beta_5+4\beta_6+\beta_7\right)\epsilon_{r\theta}+2\left(2\beta_5\epsilon_{\varphi\varphi}+\beta_7\left(\epsilon_{rr}+\epsilon_{\theta\theta}\right)\right)\sin 2\theta\\&+2\left(2\beta_5+4\beta_6-\beta_7\right)\epsilon_{r\theta}\cos 4\theta+\left(2\beta_5+4\beta_6-\beta_7\right)\left(\epsilon_{rr}-\epsilon_{\theta\theta}\right)\sin 4\theta\Big]\\&+2\sin 2\varphi\Big[\left(2\beta_5-4\beta_6-\beta_7\right)\left(\epsilon_{\varphi r}\cos\theta+\epsilon_{\theta\varphi}\sin\theta\right)+\left(2\beta_5+4\beta_6-\beta_7\right)\left(\epsilon_{\theta\varphi}\sin 3\theta-\epsilon_{\varphi r}\cos 3\theta\right)\Big]\\&-4\beta_4\sin 4\varphi\Big[\epsilon_{\varphi r}(\cos\theta-\cos 3\theta)+\epsilon_{\theta\varphi}(\sin\theta+\sin 3\theta)\Big],\end{aligned} \tag{22}$$

$$\begin{aligned}\sigma_{\theta\varphi} &= \left(2\alpha_2+\beta_1-\beta_3\right)\epsilon_{\theta\varphi}+\left(\beta_1+2\beta_2-\beta_3\right)\left(\epsilon_{\theta\varphi}\cos 2\theta+\epsilon_{\varphi r}\sin 2\theta\right)+8\beta_6\cos 2\varphi\Big[-\epsilon_{\theta\varphi}+\epsilon_{\theta\varphi}\cos 2\theta\\ &+\epsilon_{\varphi r}\sin 2\theta\Big]-8\beta_4\cos 4\varphi\Big[\epsilon_{\theta\varphi}+\epsilon_{\theta\varphi}\cos 2\theta+\epsilon_{\varphi r}\sin 2\theta\Big]+\sin 2\varphi\Big[2\left(2\beta_5-4\beta_6-\beta_7\right)\epsilon_{r\theta}\sin\theta\\ &+\left(\left(-2\beta_5-4\beta_6-3\beta_7\right)\epsilon_{\theta\theta}-4\beta_7\epsilon_{\varphi\varphi}+\left(-6\beta_5+4\beta_6-\beta_7\right)\epsilon_{rr}\right)\cos\theta+2\left(2\beta_5+4\beta_6-\beta_7\right)\epsilon_{r\theta}\sin 3\theta\\ &-\left(2\beta_5+4\beta_6-\beta_7\right)\left(\epsilon_{rr}-\epsilon_{\theta\theta}\right)\cos 3\theta\Big]+2\beta_4\sin 4\varphi\Big[\left(4\epsilon_{\varphi\varphi}-\epsilon_{rr}-\epsilon_{\theta\theta}\right)\cos\theta+\left(\epsilon_{rr}-3\epsilon_{\theta\theta}\right)\cos 3\theta\\ &-2\epsilon_{r\theta}(\sin\theta+\sin 3\theta)\Big],\end{aligned} \tag{23}$$

$$\begin{aligned}\sigma_{\varphi r} &= \left(2\alpha_2+\beta_1-\beta_3\right)\epsilon_{\varphi r}-\left(\beta_1+2\beta_2-\beta_3\right)\left(\epsilon_{\varphi r}\cos 2\theta-\epsilon_{\theta\varphi}\sin 2\theta\right)-8\beta_6\cos 2\varphi\Big[\epsilon_{\varphi r}+\epsilon_{\varphi r}\cos 2\theta\\ &-\epsilon_{\theta\varphi}\sin 2\theta\Big]-8\beta_4\cos 4\varphi\Big[\epsilon_{\varphi r}-\epsilon_{\varphi r}\cos 2\theta+\epsilon_{\theta\varphi}\sin 2\theta\Big]+\sin 2\varphi\Big[2\left(2\beta_5-4\beta_6-\beta_7\right)\epsilon_{r\theta}\cos\theta\\ &-2\left(2\beta_5+4\beta_6-\beta_7\right)\epsilon_{\theta r}\cos 3\theta-\left(\left(-6\beta_5+4\beta_6-\beta_7\right)\epsilon_{\theta\theta}-4\beta_7\epsilon_{\varphi\varphi}+\left(-2\beta_5-4\beta_6-3\beta_7\right)\epsilon_{rr}\right)\sin\theta\\ &-\left(2\beta_5+4\beta_6-\beta_7\right)\left(\epsilon_{rr}-\epsilon_{\theta\theta}\right)\sin 3\theta\Big]-2\beta_4\sin 4\varphi\Big[\left(3\epsilon_{rr}+\epsilon_{\theta\theta}-4\epsilon_{\varphi\varphi}\right)\sin\theta-\left(\epsilon_{rr}-\epsilon_{\theta\theta}\right)\sin 3\theta\\ &+2\epsilon_{r\theta}\left(\cos\theta-\cos 3\theta\right)\Big],\end{aligned} \tag{24}$$

where the strains in spherical coordinates are

$$\begin{aligned}&\epsilon_{rr}=\frac{\partial u_r}{\partial r},\quad \epsilon_{\varphi\varphi}=\frac{1}{r\sin\theta}\frac{\partial u_\varphi}{\partial\varphi}+\frac{\cot\theta}{r}u_\theta+\frac{u_r}{r},\\ &\epsilon_{\theta\theta}=\frac{1}{r}\frac{\partial u_\theta}{\partial\theta}+\frac{u_r}{r},\quad \epsilon_{\theta\varphi}=\frac{1}{2r}\left(\frac{\partial u_\varphi}{\partial\theta}-\cot\theta u_\varphi+\frac{1}{\sin\theta}\frac{\partial u_\theta}{\partial\varphi}\right),\\ &\epsilon_{\varphi r}=\frac{1}{2}\left(\frac{1}{r\sin\theta}\frac{\partial u_r}{\partial\varphi}+\frac{\partial u_\varphi}{\partial r}-\frac{u_\varphi}{r}\right),\quad \epsilon_{r\theta}=\frac{1}{2}\left(\frac{\partial u_\theta}{\partial r}-\frac{u_\theta}{r}+\frac{1}{r}\frac{\partial u_r}{\partial\theta}\right).\end{aligned} \tag{25}$$

Here, $\alpha_1,\alpha_2,\beta_1,\beta_2,\beta_3,\beta_4,\beta_5,\beta_6$ and β_7 are new stiffness constants defined as

$$\begin{aligned}&\alpha_1=\frac{1}{64}\left(3C_{11}+2C_{12}+24C_{13}+3C_{22}+24C_{23}+8C_{33}+4C_{66}-16C_{55}-16C_{44}\right),\\ &\alpha_2=\frac{1}{64}\left(3C_{11}+2C_{12}-8C_{13}+3C_{22}-8C_{23}+8C_{33}+4C_{66}+16C_{55}+16C_{44}\right),\\ &\beta_1=\frac{1}{32}\left(3C_{11}+2C_{12}+3C_{22}-8C_{33}+4C_{66}\right),\\ &\beta_2=\frac{1}{64}\left(3C_{11}+2C_{12}-8C_{13}+3C_{22}-8C_{23}+8C_{33}+4C_{66}-16C_{55}-16C_{44}\right),\\ &\beta_3=\frac{1}{16}\left(C_{11}+6C_{12}-4C_{13}+C_{22}-4C_{23}-4C_{66}\right),\\ &\beta_4=\frac{1}{64}\left(C_{11}-2C_{12}+C_{22}-4C_{66}\right),\qquad \beta_5=\frac{1}{16}\left(C_{13}-C_{23}\right),\\ &\beta_6=\frac{1}{16}\left(C_{55}-C_{44}\right),\qquad \beta_7=\frac{1}{16}\left(C_{11}-C_{22}\right).\end{aligned} \tag{26}$$

In the isotropic limit the first two become the Lamé constants λ_1 and μ_1 of the sphere whereas the other seven vanish. Substituting (19)–(25) into (16)–(18), gives the governing equations of the displacement field; however, this leads to very large equations which are not given. Due to the trigonometric functions in θ and φ there are extensive couplings between different orders and degrees when expansions in spherical harmonics are later performed.

To solve the scattering problem the scattered wave outside the sphere and the interior wave inside the sphere are to be determined given the incident wave. Of course, expanding the displacement field inside the sphere in terms of the spherical vector wave functions does not satisfy the governing equations of an anisotropic medium. Instead, the vector spherical harmonics are appropriate for the expansion of the displacement inside the sphere since the displacement and stress fields outside the sphere are also in terms of these functions and this facilitates the application of the boundary conditions. Therefore, the displacement field inside the sphere is expanded as

$$\boldsymbol{u}_1(r,\theta,\varphi)=\sum_{\tau\sigma ml}F_{\tau\sigma ml}(r)\boldsymbol{A}_{\tau\sigma ml}(\theta,\varphi). \tag{27}$$

where $l=1,2,\ldots$ for $\tau=1,2$ and $l=0,1,\ldots$ for $\tau=3$. The r dependent coefficients $F_{\tau\sigma ml}(r)$ are expanded in power series in r. By considering the regularity condition at the center of the sphere, these expansions are

$$F_{1\sigma ml}(r)=\sum_{j=l,l+2,\ldots}^{\infty}f_{1\sigma ml,j}r^j, \tag{28}$$

$$F_{2\sigma ml}(r)=\sum_{j=l-1,l+1,\ldots}^{\infty}f_{2\sigma ml,j}r^j, \tag{29}$$

$$F_{3\sigma ml}(r)=\sum_{j=l-1,l+1,\ldots}^{\infty}f_{3\sigma ml,j}r^j, \tag{30}$$

in which $f_{3\sigma m0,-1}=0$. Here, $f_{\tau\sigma ml,j}$ are the unknown coefficients inside the sphere.

The governing equations Eqs. (16)–(18) provide recursion relations among these unknown coefficients inside the sphere. To derive these, the three governing equations Eqs. (16)–(18) are considered as one vector valued function and are expanded in terms of the vector spherical harmonics

$$\sum_{\tau\sigma ml}H_{\tau\sigma ml}(r)\boldsymbol{A}_{\tau\sigma ml}(\theta,\varphi)=\boldsymbol{0}. \tag{31}$$

Table 1
Table of couplings among the partial waves in the Rayleigh limit.

P-SV σml	Partial P waves $\tau = 3$	Partial SV waves $\tau = 2$	Partial SH waves $\tau = 1$	Sec.
ooo	$\boldsymbol{A}_{3o11}, (\boldsymbol{A}_{3o13}, \boldsymbol{A}_{3o33})$	$\boldsymbol{A}_{2o11}, (\boldsymbol{A}_{2o13}, \boldsymbol{A}_{2o33})$	$(\boldsymbol{A}_{1e12})$	4.1
eoo	$\boldsymbol{A}_{3e11}, (\boldsymbol{A}_{3e13}, \boldsymbol{A}_{3e33})$	$\boldsymbol{A}_{2e11}, (\boldsymbol{A}_{2e13}, \boldsymbol{A}_{2e33})$	$(\boldsymbol{A}_{1o12})$	4.1
oeo	$(\boldsymbol{A}_{3o23})$	$(\boldsymbol{A}_{2o23})$	$(\boldsymbol{A}_{1e02}, \boldsymbol{A}_{1e22})$	4
eeo	$\boldsymbol{A}_{3e01}, (\boldsymbol{A}_{3e03}, \boldsymbol{A}_{3e23})$	$\boldsymbol{A}_{2e01}, (\boldsymbol{A}_{2e03}, \boldsymbol{A}_{2e23})$	$(\boldsymbol{A}_{1o22})$	4.1
ooe	$\boldsymbol{A}_{3o12}, (\boldsymbol{A}_{3o14}, \boldsymbol{A}_{3o34})$	$\boldsymbol{A}_{2o12}, (\boldsymbol{A}_{2o14}, \boldsymbol{A}_{2o34})$	$(\boldsymbol{A}_{1e11}, \boldsymbol{A}_{1e13}, \boldsymbol{A}_{1e33})$	4.2
eoe	$\boldsymbol{A}_{3e12}, (\boldsymbol{A}_{3e14}, \boldsymbol{A}_{3e34})$	$\boldsymbol{A}_{2e12}, (\boldsymbol{A}_{2e14}, \boldsymbol{A}_{2e34})$	$(\boldsymbol{A}_{1o11}, \boldsymbol{A}_{1o13}, \boldsymbol{A}_{1o33})$	4.3
oee	$\boldsymbol{A}_{3o22}, (\boldsymbol{A}_{3o24}, \boldsymbol{A}_{3o44})$	$\boldsymbol{A}_{2o22}, (\boldsymbol{A}_{2o24}, \boldsymbol{A}_{2o44})$	$(\boldsymbol{A}_{1e01}, \boldsymbol{A}_{1e03}, \boldsymbol{A}_{1e23})$	4.4
eee	$\boldsymbol{A}_{3e00}, \boldsymbol{A}_{3e02}, \boldsymbol{A}_{3e22}$ $(\boldsymbol{A}_{3e04}, \boldsymbol{A}_{3e24}, \boldsymbol{A}_{3e44})$	$\boldsymbol{A}_{2e02}, \boldsymbol{A}_{2e22}$ $(\boldsymbol{A}_{2e04}, \boldsymbol{A}_{2e24}, \boldsymbol{A}_{2e44})$	$(\boldsymbol{A}_{1o23})$	4.5

Here, $H_{\tau\sigma ml}$ is the scalar product of a vector spherical harmonic and the governing vector equation. The orthogonality of the vector spherical harmonics means that all these coefficients, which are power series in r, must vanish so that

$$H_{\tau\sigma ml}(r) = 0 \qquad \text{for all} \quad \tau, \sigma, m, l. \tag{32}$$

As the powers of r are linearly independent, the coefficient in front of every power of r must vanish, which provides the recursion relations among the unknown coefficients inside the sphere and leaves only one unknown for each partial wave. The general explicit expression of these recursion relations is complicated and is not given. The recursion relations also give couplings among the partial waves. Such coupling is discussed in detail for a sphere with transversely isotropic [28] and cubic [29] material properties. For the orthorhombic sphere, there is a similar coupling among the partial waves as for the cubic material, but with extra couplings of $|m \pm 2|$ partial waves with m and $|m \pm 4|$. This is expected as there are trigonometric functions of order 2φ in the strain–stress relations Eqs. (19)–(24) (which are absent in the cubic case).

To find all the unknown expansion coefficients inside and outside the sphere there remains to apply the boundary conditions on the sphere. Assuming the sphere to be perfectly welded with the surrounding, the displacement and normal traction must be continuous at the surface of the sphere $r = a$. The displacement field outside and inside of the sphere (Eqs. (13) and (27)) are expanded in terms of the vector spherical harmonics and using the orthonormality of the vector spherical harmonics application of the boundary conditions is straightforward. For the traction boundary condition, the radial traction just inside the sphere is expanded in terms of the vector spherical harmonics as

$$\boldsymbol{t}_1^{(r)}(a, \theta, \varphi) = \sum_{\tau\sigma ml} G_{\tau\sigma ml} \boldsymbol{A}_{\tau\sigma ml}(\theta, \varphi), \tag{33}$$

where $G_{\tau\sigma ml}$ is the scalar product of the radial traction vector and vector spherical harmonics of order τ, σ, m and l. Such an expansion of the traction inside the sphere together with the traction outside the sphere (Eqs. (9)–(12)) makes it straightforward to apply the traction boundary condition. It is noted that $G_{\tau\sigma ml}$ shows the same coupling among the coefficients $f_{\tau\sigma ml,j}$ as in $H_{\tau\sigma ml}(r)$.

The boundary conditions and the recursion relations give all the equations needed to determine all expansion coefficients and thereby the fields outside and inside the sphere. It is, in particular, possible to determine the **T** matrix elements. Due to their complexity, explicit expressions for all these equations cannot be stated, but for low frequencies it is possible to obtain explicit expressions for the leading order **T** matrix elements, and for higher frequencies it is possible to solve the equations numerically.

In the low frequency limit it is sufficient to expand the displacement field to power 3 in r. With such a truncation in Eqs. (28)–(30), 64 partial waves remain for the displacement field inside the sphere, which are listed in Table 1. The continuity condition of displacement and traction for each vector spherical harmonic leads to a large system of equations to be solved. However, materials with orthorhombic symmetry have three orthogonal symmetry planes, which leads to a decoupling into eight independent subproblems. Table 1 presents the eight distinct sets of decoupled partial waves at low frequencies. In the low frequency limit, it has been established for cubic materials that the leading order **T** matrix elements for SH waves are of higher order than those for P and SV waves [28] and this is true also for orthorhombic materials. Therefore, it is adequate to only consider P and SV waves ($\tau = 2$ and 3). Additionally, only incident partial waves with orders $l = 0$, 1, and 2 are needed for determining the leading order **T** matrix elements at low frequencies. Thus all partial waves with $\tau = 1$ and $l \geq 3$ inside the sphere (which are enclosed in parentheses in Table 1) are not of leading order at low frequencies. The subsequent section presents the leading order **T** matrix elements in the low frequency limit for each of the eight sets.

4. Low frequency T matrix elements

In this section all the leading order **T** matrix elements in the low frequency limit are explicitly stated. To keep the exposition brief, some details of the calculations are only explained for the first case with odd–odd–odd P-SV waves, and for the other cases only the truncated displacement expansion and the **T** matrix elements are presented. As shown in Table 1 for the odd–even–odd case there is no leading order **T** matrix element in the low frequency limit, so the other seven cases remain. For more calculational details see Jafarzadeh et al. [28,29] where the **T** matrix elements for a sphere with transversely isotropic and cubic material properties are derived, respectively.

4.1. Odd–odd–odd P-SV waves

For the case with odd–odd–odd P-SV waves, $\sigma = o$, $m = 1$, and $l = 1$, the low frequency displacement field expansion is

$$\boldsymbol{u}_1(r, \theta, \varphi) = F_{2o11}(r)\mathbf{A}_{2o11}(\theta, \varphi) + F_{3o11}(r)\mathbf{A}_{3o11}(\theta, \varphi), \tag{34}$$

where

$$F_{2o11}(r) = f_{2o11,0} + f_{2o11,2}r^2, \quad F_{3o11}(r) = f_{3o11,0} + f_{3o11,2}r^2. \tag{35}$$

As in Section 3, the equations of motion are projected onto $\mathbf{A}_{2o11}(\theta,\varphi)$ and $\mathbf{A}_{3o11}(\theta,\varphi)$ with only the two lowest order in r retained. The resulting two distinct equations are solved to give the two recursion relations

$$f_{2o11,0} = \sqrt{2} f_{3o11,0}, \qquad f_{3o11,2} = \frac{\sqrt{2}\left(2\alpha_1 - 2\alpha_2 - \beta_1 - 2\beta_2 + 3\beta_3 - 8\beta_5 + 8\beta_6\right) f_{2o11,2} - 2\rho_1\omega^2 f_{3o11,0}}{2\left(4\alpha_1 + 6\alpha_2 + 5\beta_1 + \beta_3 - 8\beta_5 - 8\beta_6 - 16\beta_7\right)}. \tag{36}$$

Thus, two unknowns remain inside the sphere, and the unknowns outside the sphere are h_{2o01} and h_{3o01}. These are found by using the continuity of displacement and traction for $\tau = 2$ and $\tau = 3$ with $l = 1$ (again projecting), and the $\mathbf{T}$ matrix elements are calculated as

$$\begin{aligned}
T_{2o11,2o11} &= -\frac{2}{9} i \left(k_s a\right)^3 \left(1 - \frac{\rho_1}{\rho}\right), \\
T_{3o11,2o11} &= T_{2o01,3o01} = -\frac{\sqrt{2}}{9} i \left(\sqrt{k_p k_s}\, a\right)^3 \left(1 - \frac{\rho_1}{\rho}\right), \\
T_{3o11,3o11} &= -\frac{1}{9} i \left(k_p a\right)^3 \left(1 - \frac{\rho_1}{\rho}\right).
\end{aligned} \tag{37}$$

The $\mathbf{T}$ matrix elements only depend on the density of the sphere, and are independent of its elasticity constants. Thus, these elements are the same for any type of spherical inclusion. This is reasonable since the $l = 1$ case for low frequencies is related to the rigid body translation of the sphere. Consequently, all other $\mathbf{T}$ matrix elements of order $l = 1$ are the same regardless of their parity with respect to σ and m and the following relations thus follows for the even–odd–odd and even–even–odd cases

$$\begin{aligned}
&T_{2o11,2o11} = T_{2e11,2e11} = T_{2e01,2e01}, \\
&T_{3o11,2o11} = T_{2o11,3o11} = T_{3e11,2e11} = T_{2e11,3e11} = T_{3e01,2e01} = T_{2e01,3e01}, \\
&T_{3o11,3o11} = T_{3e11,3e11} = T_{3e01,3e01}.
\end{aligned} \tag{38}$$

In the following subsections only the suitably truncated displacement field and the $\mathbf{T}$ matrix elements for the other cases are stated.

4.2. Odd–odd–even P-SV waves

This case has $\sigma = o$, $m = 1$, and $l = 2$ and the displacement expansion is

$$\boldsymbol{u}_1(r,\theta,\varphi) = F_{2o12}(r)\mathbf{A}_{2o12}(\theta,\varphi) + F_{3o12}(r)\mathbf{A}_{3o12}(\theta,\varphi) \tag{39}$$

The $\mathbf{T}$ matrix elements become

$$\begin{aligned}
T_{2o12,2o12} &= -2i \left(k_s a\right)^3 \frac{\left(C_{55} - \mu\right)(\lambda + 2\mu)}{2C_{55}(3\lambda + 8\mu) + \mu(9\lambda + 14\mu)}, \\
T_{3o12,2o12} &= T_{2o12,3o12} = -2\sqrt{\frac{2}{3}} i \left(\sqrt{k_p k_s}\, a\right)^3 \frac{\left(C_{55} - \mu\right)\sqrt{\mu(\lambda + 2\mu)}}{2C_{55}(3\lambda + 8\mu) + \mu(9\lambda + 14\mu)}, \\
T_{3o12,3o12} &= -\frac{4}{3} i \left(k_p a\right)^3 \frac{\mu\left(C_{55} - \mu\right)}{2C_{55}(3\lambda + 8\mu) + \mu(9\lambda + 14\mu)}.
\end{aligned} \tag{40}$$

4.3. Even–odd–even P-SV waves

This case has $\sigma = e$, $m = 1$, and $l = 2$ and the displacement expansion is

$$\boldsymbol{u}_1(r,\theta,\varphi) = F_{2e12}(r)\mathbf{A}_{2e12}(\theta,\varphi) + F_{3e12}(r)\mathbf{A}_{3e12}(\theta,\varphi) \tag{41}$$

The $\mathbf{T}$ matrix elements become

$$\begin{aligned}
T_{2e12,2e12} &= -2i \left(k_s a\right)^3 \frac{\left(C_{44} - \mu\right)(\lambda + 2\mu)}{2C_{44}(3\lambda + 8\mu) + \mu(9\lambda + 14\mu)}, \\
T_{3e12,2e12} &= T_{2e12,3e12} = -2\sqrt{\frac{2}{3}} i \left(\sqrt{k_p k_s}\, a\right)^3 \frac{\left(C_{44} - \mu\right)\sqrt{\mu(\lambda + 2\mu)}}{2C_{44}(3\lambda + 8\mu) + \mu(9\lambda + 14\mu)}, \\
T_{3e12,3e12} &= -\frac{4}{3} i \left(k_p a\right)^3 \frac{\mu\left(C_{44} - \mu\right)}{2C_{44}(3\lambda + 8\mu) + \mu(9\lambda + 14\mu)}.
\end{aligned} \tag{42}$$

4.4. Odd–even–even P-SV waves

This case has $\sigma = o$, $m = 2$, and $l = 2$ and the displacement expansion is

$$\boldsymbol{u}_1(r,\theta,\varphi) = F_{2o22}(r)\mathbf{A}_{2o22}(\theta,\varphi) + F_{3o22}(r)\mathbf{A}_{3o22}(\theta,\varphi). \tag{43}$$

The $\mathbf{T}$ matrix elements become

$$\begin{aligned}
T_{2o22,2o22} &= -2i \left(k_s a\right)^3 \frac{\left(C_{66} - \mu\right)(\lambda + 2\mu)}{2C_{66}(3\lambda + 8\mu) + \mu(9\lambda + 14\mu)}, \\
T_{3o22,2o22} &= T_{2o22,3o22} = -2\sqrt{\frac{2}{3}} i \left(\sqrt{k_p k_s}\, a\right)^3 \frac{\left(C_{66} - \mu\right)\sqrt{\mu(\lambda + 2\mu)}}{2C_{66}(3\lambda + 8\mu) + \mu(9\lambda + 14\mu)}, \\
T_{3o22,3o22} &= -\frac{4}{3} i \left(k_p a\right)^3 \frac{\mu\left(C_{66} - \mu\right)}{2C_{66}(3\lambda + 8\mu) + \mu(9\lambda + 14\mu)}.
\end{aligned} \tag{44}$$

It is noticed that the three last cases, all with only $l = 2$ (and with no coupling to $l = 0$), are very similar, it is just to exchange the three shear moduli C_{44}, C_{55}, C_{66}. All these **T** matrix elements are independent of all the other stiffness constants. In the cubic and transversely isotropic cases, with $C_{44} = C_{55} = C_{66}$ and $C_{44} = C_{55}, C_{66} = (C_{11} - C_{12})/2$, respectively, the same **T** matrix elements are obtained by Jafarzadeh et al. [28,29].

4.5. Even–even–even P-SV waves

This case has $\sigma = e$, $m = 0, 2$, and $l = 0, 2$, and is by far the most complicated and has the displacement expansion

$$\begin{aligned}\boldsymbol{u}_1(r,\theta,\varphi) &= F_{2e02}(r)\mathbf{A}_{2e02}(\theta,\varphi) + F_{2e22}(r)\mathbf{A}_{2e22}(\theta,\varphi) + F_{3e00}(r)\mathbf{A}_{3e00}(\theta,\varphi) + F_{3e02}(r)\mathbf{A}_{3e02}(\theta,\varphi)\\ &+ F_{3e22}(r)\mathbf{A}_{3e22}(\theta,\varphi).\end{aligned} \tag{45}$$

After very long calculations the **T** matrix elements become

$$\begin{aligned}
T_{3e00,3e00} &= -\frac{1}{3} i \left(k_p a\right)^3 \left(1 - (\lambda + 2\mu)\frac{N_{00,00}}{D}\right),\\
T_{2e02,3e00} &= T_{3e00,2e02} = \sqrt{\frac{5}{6}} i \left(\sqrt{k_p k_s}\, a\right)^3 (\lambda + 2\mu)\sqrt{\mu(\lambda + 2\mu)}\frac{N_{00,02}}{D},\\
T_{3e02,3e00} &= T_{3e00,3e02} = \frac{\sqrt{5}}{3} i \left(k_p a\right)^3 \mu(\lambda + 2\mu)\frac{N_{00,02}}{D},\\
T_{2e22,3e00} &= T_{3e00,2e22} = \sqrt{\frac{5}{2}} i \left(\sqrt{k_p k_s}\, a\right)^3 (\lambda + 2\mu)\sqrt{\mu(\lambda + 2\mu)}\frac{N_{02,02}}{D},\\
T_{3e22,3e00} &= T_{3e00,3e22} = \sqrt{\frac{5}{3}} i \left(k_p a\right)^3 \mu(\lambda + 2\mu)\frac{N_{02,02}}{D},\\
T_{2e22,2e02} &= T_{2e02,2e22} = \frac{5\sqrt{3}}{2} i \left(k_s a\right)^3 \mu(\lambda + 2\mu)^2\frac{N_{02,22}}{D},\\
T_{3e22,2e02} &= T_{2e02,3e22} = T_{2e22,3e02} = T_{3e02,2e22} = \frac{5}{\sqrt{2}} i \left(\sqrt{k_p k_s}\, a\right)^3 \mu(\lambda + 2\mu)\sqrt{\mu(\lambda + 2\mu)}\frac{N_{02,22}}{D},\\
T_{3e22,3e02} &= T_{3e02,3e22} = \frac{5}{\sqrt{3}} i \left(k_p a\right)^3 \mu^2(\lambda + 2\mu)\frac{N_{02,22}}{D},\\
T_{2e02,2e02} &= -\frac{1}{2} i \left(k_s a\right)^3 (\lambda + 2\mu)\frac{N_{00,22}}{D},\\
T_{3e02,2e02} &= T_{2e02,3e02} = -\frac{1}{\sqrt{6}} i \left(\sqrt{k_p k_s}\, a\right)^3 \sqrt{\mu(\lambda + 2\mu)}\frac{N_{00,22}}{D},\\
T_{3e02,3e02} &= -\frac{1}{3} i \left(k_p a\right)^3 \mu\frac{N_{00,22}}{D},\\
T_{2e22,2e22} &= -\frac{1}{2} i \left(k_s a\right)^3 (\lambda + 2\mu)\frac{N_{22,22}}{D},\\
T_{3e22,3e22} &= T_{3e22,2e22} = -\frac{1}{\sqrt{6}} i \left(\sqrt{k_p k_s}\, a\right)^3 \sqrt{\mu(\lambda + 2\mu)}\frac{N_{22,22}}{D},\\
T_{3e22,3e22} &= -\frac{1}{3} i \left(k_p a\right)^3 \mu\frac{N_{22,22}}{D},
\end{aligned} \tag{46}$$

where D is the denominator and $N_{mm',ll'}$ is the numerator for the **T** matrix elements related to the scattered wave of order m', l' due to the incident wave of order m, l, and vice versa. $N_{mm',ll'}$ and D can be expressed in terms of the elasticity constants

$$\begin{aligned}
N_{00,00} &= -2\left(C_{11} - C_{12} - C_{13} + C_{22} - C_{23} + C_{33}\right)\mu(9\lambda + 14\mu)(3\lambda + 8\mu) + \left(\, C_{12}^2 - 2C_{13}C_{12} - 2C_{23}C_{12}\right.\\
&+ 2C_{33}C_{12} + C_{13}^2 + C_{23}^2 - C_{11}C_{22} + 2C_{13}C_{22} + 2C_{11}C_{23} - 2C_{13}C_{23} - C_{11}C_{33} - C_{22}C_{33}\left.\,\right)(3\lambda + 8\mu)^2\\
&- 3\mu^2(9\lambda + 14\mu)^2,\\
N_{00,02} &= \left(\, -2C_{12}^2 + C_{13}C_{12} + C_{23}C_{12} + 2C_{33}C_{12} + C_{13}^2 + C_{23}^2 + 2C_{11}C_{22} - C_{13}C_{22} - C_{11}C_{23}\right.\\
&- \left.2C_{13}C_{23} - C_{11}C_{33} - C_{22}C_{33}\,\right)(3\lambda + 8\mu) + \left(C_{11} + 2C_{12} - C_{13} + C_{22} - C_{23} - 2C_{33}\right)\mu(9\lambda + 14\mu),\\
N_{02,02} &= \left(C_{13}^2 - C_{12}C_{13} - C_{22}C_{13} - C_{23}^2 + C_{11}C_{23} + C_{12}C_{23} - C_{11}C_{33} + C_{22}C_{33}\right)(3\lambda + 8\mu)\\
&- \left(C_{11} + C_{13} - C_{22} - C_{23}\right)\mu(9\lambda + 14\mu),\\
N_{02,22} &= C_{13}^2 + 2C_{12}C_{13} + 2C_{22}C_{13} - C_{23}^2 - 2C_{11}C_{23} - 2C_{12}C_{23} - C_{11}C_{33} + C_{22}C_{33}\\
&+ \left(-4C_{11} + 8C_{13} + 4C_{22} - 8C_{23}\right)\mu,
\end{aligned} \tag{47}$$

$$\begin{aligned}
N_{00,22} &= -4\mu^2\left(-2C_{13} - 2C_{23} + C_{33} - 4\right)(9\lambda + 14\mu) + 2(3\lambda + 8\mu)\left(\, C_{33}C_{12}^2 - 2C_{13}C_{23}C_{12} + C_{11}C_{23}^2\right.\\
&+ C_{13}^2C_{22} - C_{11}C_{22}C_{33} - 4\mu\left(C_{12}C_{13} - C_{22}C_{13} - C_{11}C_{23} + C_{12}C_{23}\right) + 4\mu^2\left(C_{11} - 2C_{12} + C_{22}\right)\left.\,\right)\\
&- \mu\Big(2\left(C_{12}C_{33} - C_{13}C_{23}\right)(3\lambda - 2\mu) + 15\left(-C_{13}^2 - C_{23}^2 + C_{11}C_{33} + C_{22}C_{33}\right)(\lambda + 2\mu)\Big),
\end{aligned}$$

$$
\begin{aligned}
N_{22,22} &= N_{00,22} + 10\mu(\lambda+2\mu)\,\big(\,\big(-4C_{11}+16C_{12}-8C_{13}-4C_{22}-8C_{23}+8C_{33}\big)\,\mu + 2C_{12}^2 + 2C_{13}C_{12} \\
&\quad + 2C_{23}C_{12} + 4C_{33}C_{12} - C_{13}^2 - C_{23}^2 - 2C_{11}C_{22} - 2C_{13}C_{22} - 2C_{11}C_{23} - 4C_{13}C_{23} + C_{11}C_{33} + C_{22}C_{33}\,\big), \\
D &= \mu^2(9\lambda+14\mu)\,\big(2\,\big(C_{12}+C_{13}+C_{23}\big)\,(\lambda+6\mu) - \big(C_{11}+C_{22}+C_{33}\big)\,(11\lambda+26\mu)\big) \\
&\quad + 2\mu(3\lambda+8\mu)\,\Big(\,5\,\big(C_{12}^2+C_{13}^2+C_{23}^2-C_{11}C_{22}-C_{11}C_{33}-C_{22}C_{33}\big)\,(\lambda+2\mu) \\
&\quad - \big(C_{12}C_{13}-C_{22}C_{13}+C_{23}C_{13}-C_{11}C_{23}+C_{12}C_{23}-C_{12}C_{33}\big)\,(\lambda+6\mu)\,\Big) \\
&\quad + \big(C_{33}C_{12}^2 - 2C_{13}C_{23}C_{12} + C_{11}C_{23}^2 + C_{13}^2C_{22} - C_{11}C_{22}C_{33}\big)\,(3\lambda+8\mu)^2 - 4\mu^3(9\lambda+14\mu)^2.
\end{aligned}
$$

It is noticed that these **T** matrix elements are all independent of the shear moduli C_{44}, C_{55}, and C_{66}. In the isotropic limit where $C_{11}=C_{22}=C_{33}=\lambda_1+2\mu_1, C_{12}=C_{13}=C_{23}=\lambda_1, C_{44}=C_{55}=C_{66}=\mu_1$ (λ_1 and μ_1 being the Lamé constants of the isotropic sphere), the transversely isotropic limit where $C_{11}=C_{22}, C_{12}=C_{13}, C_{44}=C_{55}, C_{66}=(C_{11}-C_{22})/2$, and the cubic limit where $C_{11}=C_{22}=C_{33}, C_{12}=C_{13}=C_{23}, C_{44}=C_{55}=C_{66}$, these **T** matrix elements are the same as the ones given by Boström [31] and Jafarzadeh et al. [28,29], respectively. These **T** matrix elements provide complete information regarding low frequency scattering in a medium with a spherical inclusion of orthorhombic symmetry.

Looking at the **T** matrix elements, the leading order ones in the low frequency limit are all imaginary. The leading order real parts of the **T** matrix elements are of higher order and require higher order expansion of the displacement field. Using the "hermitian" property of the **T** matrix [32]

$$\mathbf{T}^{\dagger}\mathbf{T} = -\mathrm{Re}\mathbf{T}, \tag{48}$$

the leading order real part of the **T** matrix elements is obtained from the leading order imaginary parts of them.

The derived **T** matrix elements are all that are of leading order at low frequencies. Low frequencies typically means $k_s a < 0.5$, but this of course depends on the accuracy required. It must also be recognized that the wave numbers of the material inside the sphere play a role, so if one of the wave numbers inside the sphere is larger this may limit the range of frequencies further. There is, on the other hand, no limit on the strength of the anisotropy. This is in contrast with the perturbative Keller approximation [33] or the diagrammatic Bourret approximation [34], which are typically used in methods like SOA, and are only valid for small anisotropy (but has no limit in frequency).

5. Polycrystalline materials

Polycrystalline materials are composed of a collection of crystals with anisotropic properties. Due to the grainy structure, propagating waves in the medium scatter and attenuate. In the case of randomly oriented, equiaxed crystals, the macroscopic behavior of the polycrystals is isotropic and homogeneous. The medium is then characterized by the effective wave numbers K_p and K_s for the longitudinal and transverse waves, respectively. The effective wave numbers are complex numbers in which the real part gives the phase velocity and the imaginary part gives the attenuation of the wave. Since the scattering depends on the frequency, the effective phase velocity and attenuation are, in general, frequency dependent. However, for very low frequencies the state in the medium is quasi-static, attenuation is small, and the wave number provides a quasi-static velocity limit of the medium. Considering that a polycrystalline material is filled with crystals, the propagating wave constantly experiences multiple events of scattering. Modeling all these events of scattering is complicated, and different simplifying assumptions are considered in the literature to study wave propagation in these materials.

Here an approach where the scattering by each crystal is regarded as taking place in the effective and isotropic medium (called the matrix) of all the other grains is followed. Multiple scattering is neglected and it is assumed that each grain encounters the same incident wave throughout the whole medium. The matrix is then a homogeneous medium with no attenuation and constant phase velocities, which can be calculated by the Voigt average. Therefore, the method is called the Single Scattering Approximation in the Voigt homogenized medium (SSA-V). The matrix is defined by the longitudinal $k_p=\sqrt{\rho/(\lambda+2\mu)}$ and transverse $k_s=\sqrt{\rho/\mu}$ wave numbers. The density ρ for a single-phase polycrystalline material is the same as the single crystal density ρ_1. The Lamé parameters are the Voigt averages of a single crystal, which have the following relation to the stiffness constants of a material with orthorhombic symmetry [35]

$$
\begin{aligned}
\lambda &= \frac{1}{15}\left(C_{11}+4C_{12}+4C_{13}+C_{22}+4C_{23}+C_{33}-2C_{44}-2C_{55}-2C_{66}\right), \\
\mu &= \frac{1}{15}\left(C_{11}-C_{12}-C_{13}+C_{22}-C_{23}+C_{33}+3C_{44}+3C_{55}+3C_{66}\right).
\end{aligned} \tag{49}
$$

By substituting the surrounding medium of each crystal with a homogenized isotropic medium, each crystal contributes to a single scattering event which can be addressed by the calculated **T** matrix elements. With these assumptions, the theory of Foldy [21], neglecting correlations among the individual scatterers [24], is used to study the effective wave numbers of the polycrystal as [28,29]

$$
\begin{aligned}
\left(\frac{K_p}{k_p}\right)^2 &= 1 - \frac{4\pi i d}{V k_p^3}\sum_{\sigma ml} T_{3\sigma ml,3\sigma ml}, \\
\left(\frac{K_s}{k_s}\right)^2 &= 1 - \frac{2\pi i d}{V k_s^3}\sum_{\substack{\tau\sigma ml \\ \tau=1,2}} T_{\tau\sigma ml,\tau\sigma ml},
\end{aligned} \tag{50}
$$

where k_p and k_s are the wave numbers of the matrix (which are the Voigt averages in the SSA-V method), and K_p and K_s are the polycrystalline effective wave numbers for longitudinal and transverse waves, respectively. $V=4\pi a^3/3$ is the volume of a single grain and d is the relative density of the grains which for a polycrystalline materials is set to be $d=1$ as the grains fill the volume. The grains in the polycrystalline material are considered to be spheres with the same radius a meaning that no distribution of grain size is considered. This is a reasonable approximation for low frequencies, for which the scattering is mainly a volume effect. The resulting complex effective wave number describes the attenuation and phase velocity of the composite medium as

$$\frac{\alpha_i}{k_i} = \mathrm{Im}\,\frac{K_i}{k_i}, \qquad \frac{C_i}{c_i} = \mathrm{Re}\,\frac{k_i}{K_i}, \tag{51}$$

where $i = p$ and s for longitudinal and transverse waves, respectively, α_i is the attenuation, c_i is the phase velocity in the matrix and C_i is the effective phase velocity.

Collecting everything, the leading order of the real and imaginary parts of the effective wavenumbers K_i becomes

$$\left(\frac{K_p}{k_p}\right)^2 = 1 + A_p + B_p i, \qquad \left(\frac{K_s}{k_s}\right)^2 = 1 + A_s + B_s i, \tag{52}$$

where the coefficients are real and given by

$$\begin{aligned}
A_p =& -\frac{4\mu\left(C_{44}-\mu\right)}{2C_{44}(3\lambda+8\mu)+\mu(9\lambda+14\mu)} - \frac{4\mu\left(C_{55}-\mu\right)}{2C_{55}(3\lambda+8\mu)+\mu(9\lambda+14\mu)} - \frac{4\mu\left(C_{66}-\mu\right)}{2C_{66}(3\lambda+8\mu)+\mu(9\lambda+14\mu)} \\
&+ \frac{1}{D}\left((\lambda+2\mu)N_{00,00} - \mu(N_{22,22}+N_{00,22})\right) + \frac{\rho_1-\rho}{\rho} - 1, \\
B_p =& \frac{(k_p a)^3}{6}\left[\left(2+3\frac{k_s^5}{k_p^5}\right)\left(\left(\frac{4\mu\left(C_{44}-\mu\right)}{2C_{44}(3\lambda+8\mu)+\mu(9\lambda+14\mu)}\right)^2 + \left(\frac{4\mu\left(C_{55}-\mu\right)}{2C_{55}(3\lambda+8\mu)+\mu(9\lambda+14\mu)}\right)^2\right.\right. \\
&+ \left(\frac{4\mu\left(C_{66}-\mu\right)}{2C_{66}(3\lambda+8\mu)+\mu(9\lambda+14\mu)}\right)^2 + \left(\frac{\mu N_{22,22}}{D}\right)^2 + \left(\frac{\mu N_{00,22}}{D}\right)^2 + 6\left(\frac{5\mu^2(\lambda+2\mu)N_{02,22}}{D}\right)^2\Big) \\
&+ 2\left(\frac{(\lambda+2\mu)N_{00,00}}{D}-1\right)^2 + 5\left(4+3\frac{k_s^5}{k_p^5}\right)\left(\left(\frac{\mu(\lambda+2\mu)N_{00,02}}{D}\right)^2 + 3\left(\frac{\mu(\lambda+2\mu)N_{02,02}}{D}\right)^2\right) \\
&\left.+ \frac{2}{3}\left(1+2\frac{k_s^3}{k_p^3}\right)\left(\frac{\rho_1-\rho}{\rho}\right)^2\right],
\end{aligned} \tag{53}$$

$$\begin{aligned}
A_s =& -\frac{3(\lambda+2\mu)\left(C_{44}-\mu\right)}{2C_{44}(3\lambda+8\mu)+\mu(9\lambda+14\mu)} - \frac{3(\lambda+2\mu)\left(C_{55}-\mu\right)}{2C_{55}(3\lambda+8\mu)+\mu(9\lambda+14\mu)} - \frac{3(\lambda+2\mu)\left(C_{66}-\mu\right)}{2C_{66}(3\lambda+8\mu)+\mu(9\lambda+14\mu)} \\
&- \frac{3(\lambda+2\mu)}{4D}\left(N_{22,22}+N_{00,22}\right) + \frac{\rho_1-\rho}{\rho}, \\
B_s =& \frac{2(k_s a)^3}{9}\left[\left(3+2\frac{k_p^5}{k_s^5}\right)\left(\left(\frac{3(\lambda+2\mu)\left(C_{44}-\mu\right)}{2C_{44}(3\lambda+8\mu)+\mu(9\lambda+14\mu)}\right)^2 + \left(\frac{3(\lambda+2\mu)\left(C_{55}-\mu\right)}{2C_{55}(3\lambda+8\mu)+\mu(9\lambda+14\mu)}\right)^2\right.\right. \\
&+ \left(\frac{3(\lambda+2\mu)\left(C_{66}-\mu\right)}{2C_{66}(3\lambda+8\mu)+\mu(9\lambda+14\mu)}\right)^2 + \left(\frac{3(\lambda+2\mu)N_{22,22}}{4D}\right)^2 + \left(\frac{3(\lambda+2\mu)N_{00,22}}{4D}\right)^2 \\
&+ 6\left(\frac{15\mu(\lambda+2\mu)^2 N_{02,22}}{4D}\right)^2\Big) + 10\frac{k_p^5}{k_s^5}\left(\left(\frac{3(\lambda+2\mu)^2 N_{00,02}}{4D}\right)^2 + 3\left(\frac{3(\lambda+2\mu)^2 N_{02,02}}{4D}\right)^2\right) \\
&\left.+ \frac{1}{2}\left(2+\frac{k_p^3}{k_s^3}\right)\left(\frac{\rho_1-\rho}{\rho}\right)^2\right].
\end{aligned} \tag{54}$$

In the low frequency limit the parameters A_i and B_i are small and the normalized attenuation and phase velocity can be approximated with good accuracy as

$$\frac{\alpha_i}{k_i} = \frac{B_i}{2}, \qquad \frac{c_i}{C_i} = 1 + \frac{A_i}{2}. \tag{55}$$

These relations confirm the frequency dependence of attenuation and phase velocity at low frequencies, where the phase velocity is independent of the frequency and the attenuation depends on the fourth power of the frequency (or wave number). As mentioned, the frequency independent phase velocities at low frequencies provide macroscopic static properties of the polycrystal.

In the method just presented the matrix properties are determined by the Voigt average and this leads to a change in the phase velocities at low frequencies determined by A_p and A_s. Ideally this change should vanish (as it does in the case of isotropy), so nonzero A_p and A_s can be viewed as a measure of the degree of anisotropy, and they are henceforth used for this purpose. This also leads to another way to determine the Lamé parameters of the matrix by putting $A_p = A_s = 0$. These two equations can be rearranged to the following two nonlinear equations in λ and μ

$$\begin{aligned}
&\frac{\left(C_{44}-\mu\right)}{2C_{44}(3\lambda+8\mu)+\mu(9\lambda+14\mu)} + \frac{\left(C_{55}-\mu\right)}{2C_{55}(3\lambda+8\mu)+\mu(9\lambda+14\mu)} + \frac{\left(C_{66}-\mu\right)}{2C_{66}(3\lambda+8\mu)+\mu(9\lambda+14\mu)} \\
&+ \frac{N_{22,22}+N_{00,22}}{4D} = 0, \\
&(\lambda+2\mu)N_{00,00} - D = 0.
\end{aligned} \tag{56}$$

It seems that this system only has a single solution where both λ and μ are positive and real (there are further solutions that are not physically meaningful). The method to calculate the Lamé parameters λ and μ by Eq. (56) is here called the static-consistent (SC) average. The static-consistent average shows an exact agreement with the self-consistent average calculated by the script provided by Kube and De Jong [35]. (This article also give a comprehensive study of various anisotropy indices suggested in the literature and different averages and bounds of macroscopic homogenized static properties of polycrystals.) A modification of the SSA-V method is thus to define the matrix with the static-consistent elastic properties and this modified method is called the Single Scattering Approximation in the Static Consistent homogenized medium (SSA-SC). Such a consideration for the matrix properties is also suggested by Kube and Turner [13]). This method could be further generalized by iterating Eqs. (53) and (54) at finite frequencies, but this leads to attenuation and complex λ and μ, so this is not further investigated. In summary the present approach makes the following assumptions and approximations:

Table 2
Table of material properties, anisotropy degrees and anisotropy indices [15].

Type	Material	Voigt (GPa)		SC (GPa)		Anisotropy degree		Anistropy index	
		λ	μ	λ	μ	A_p	A_s	A^U	A^L
Orthorhombic	Co_2Se_4	68,87	55,87	69,27	55,25	4,6E−03	1,1E−02	0,11	0,05
	Enstatite	55,87	79,20	55,43	78,50	8,5E−03	8,8E−03	0,12	0,05
	Ni_2SiO_4	112,47	80,47	111,46	79,43	1,1E−02	1,3E−02	0,15	0,06
	Fe_2SiO_3	68,07	53,07	66,77	52,30	1,6E−02	1,4E−02	0,2	0,08
	Fe_2SiO_4	100,43	53,03	99,56	50,74	2,6E−02	4,3E−02	0,51	0,21
	U	55,99	88,06	56,73	84,17	3,0E−02	4,4E−02	0,49	0,2
	Ca_2Ag_4	39,20	16,20	37,73	15,38	4,4E−02	5,1E−02	0,58	0,23
	Sn_4Pd_40	74,33	42,33	76,92	36,76	5,3E−02	1,3E−01	2,13	0,78
	Mo_4O_{10}	91,80	42,47	84,21	38,65	8,7E−02	9,0E−02	1,28	0,47
	$Li_4Nb_4N_8$	75,80	66,13	71,76	58,43	9,3E−02	1,2E−01	1,71	0,62
	$Na_2Cu_1O_2$	46,87	30,53	50,47	22,97	1,1E−01	2,5E−01	4,1	1,33
	Te_8O_16	13,87	19,20	11,63	16,83	1,3E−01	1,2E−01	1,85	0,66
	$Na_2U_1O_4$	39,73	35,40	37,19	28,28	1,5E−01	2,1E−01	2,5	0,86
	$Sr_1Mg_6Ga_1$	18,53	15,53	13,81	10,78	2,6E−01	2,8E−01	388	10,2
Tetragonal	Mg_1Al_3	44,13	25,80	44,28	25,49	4,9E−03	1,2E−02	0,13	0,05
	Sm_4O_2	56,47	43,13	55,98	42,97	5,7E−03	3,8E−03	0,05	0,02
	Sn	47,37	19,87	48,27	18,52	2,0E−02	6,7E−02	1,34	0,53
	PDP	40,63	14,40	41,36	13,28	2,2E−02	7,7E−02	1,12	0,45
	K_2N_6	12,20	12,20	12,31	11,56	3,2E−02	5,2E−02	0,6	0,24
	Zr_1H_2	109,73	33,73	110,48	29,23	4,6E−02	1,3E−01	2,09	0,77
	Rutile	136,53	125,37	138,74	114,80	4,9E−02	8,4E−02	1,34	0,52
	NSH	8,07	12,59	8,16	11,36	7,1E−02	9,7E−02	1,55	0,58
	RDP	6,59	15,68	8,60	12,65	1,1E−01	1,9E−01	3,48	1,18
	To	24,73	29,06	28,75	22,34	1,1E−01	2,3E−01	11,32	2,64
	$Li_2C_1N_2$	40,33	20,00	37,73	16,66	1,1E−01	1,7E−01	2,53	0,88
	$Tl_2Cu_1F_4$	19,47	13,47	19,86	9,74	1,5E−01	2,8E−01	5,17	1,16
Hexagonal	α − Be	10,47	151,80	10,80	151,01	3,9E−03	5,2E−03	0,05	0,02
	α − Ti	77,73	44,07	78,20	43,36	5,8E−03	1,6E−02	0,18	0,08
	α − Co	135,27	78,27	136,34	76,64	7,5E−03	2,1E−02	0,2	0,09
	Nb_4N_4	190,93	160,43	191,08	156,75	1,4E−02	2,3E−02	0,29	0,12
	α − Tl	32,68	6,23	33,13	5,43	2,5E−02	1,3E−01	1,98	0,75
	Mn_2Sb_2	25,47	42,47	27,10	39,83	3,3E−02	6,2E−02	0,68	0,28
	Mn_2Bi_2	36,40	10,57	34,12	10,36	4,8E−02	2,0E−02	0,27	0,14
	Zn	45,93	51,27	44,50	46,80	6,9E−02	8,6E−02	1,67	0,6
	Ba_2	4,87	4,87	5,42	4,03	7,9E−02	1,8E−01	2,29	0,84
	Be_2Se_2	73,87	28,37	80,48	18,33	1,0E−01	3,5E−01	8,78	2,27
	Sr_4Si_2	20,80	16,13	23,02	12,18	1,0E−01	2,4E−01	5,17	1,58
	$Al_2Cu_2O_6$	130,87	49,70	143,14	24,79	1,4E−01	4,3E−01	196	8,26
Cubic	Al	54,92	26,42	55,01	26,29	1,6E−03	4,9E−03	0,05	0,02
	Cr	83,92	116,92	85,00	115,31	6,8E−03	1,4E−02	0,14	0,06
	Nb	137,21	39,85	138,68	37,65	1,4E−02	5,5E−02	0,63	0,26
	RbF	18,54	13,84	19,22	12,82	3,0E−02	7,4E−02	0,8	0,33
	Cu	102,24	53,84	106,34	47,69	3,9E−02	1,1E−01	1,75	0,67
	In	112,76	93,56	119,06	84,11	4,2E−02	1,0E−01	1,42	0,56
	As_1	48,40	47,40	51,72	42,42	4,7E−02	1,1E−01	1,17	0,47
	RbCl	10,34	8,84	11,23	7,50	6,5E−02	1,5E−01	1,82	0,69
	RbBr	8,15	7,83	9,07	6,44	7,9E−02	1,8E−01	2,19	0,81
	RbI	7,00	6,10	7,83	4,86	8,8E−02	2,1E−01	2,64	0,95
	Li	7,88	6,18	9,12	4,32	1,2E−01	2,9E−01	8,70	2,25
	Dy_1S_1	64,00	50,00	73,58	35,63	1,2E−01	2,9E−01	4,35	1,14

1. Each crystal is considered to be isolated from all other crystals, and they all experience the same incident wave propagating in the homogenized isotropic medium surrounding them.

2. Two assumptions are made regarding the surrounding medium: in the SSA-V approach the surrounding medium is considered to be the Voigt average of the properties of a single crystal, while in the self-consistent approach SSA-SC the surrounding medium is considered equal to the effective medium of the polycrystal in the static limit.

3. The scattered wave is studied in the far field of the surrounding homogenized medium.

4. The only statistical information of the geometrical properties of the grains considered is their effective volume, and the size distribution is neglected.

5. The explicit expressions are valid for the Rayleigh regime, where the size of the scatterers is much smaller than the wavelength of the incident wave. This is mainly due to the truncation of the **T** matrix elements to the dominant term in the low-frequency limit, which can be overcome by numerically evaluating higher orders. However, the validity of other assumptions, such as the neglect of the grain size distribution and multiple scattering, remains questionable for higher frequencies.

6. Numerical results for polycrystalline materials

This section presents numerical evaluation of the attenuation and phase velocity for the 50 different polycrystals with single-phased equiaxed crystals listed in Table 2, characterized by orthorhombic, tetragonal, hexagonal, and cubic symmetries. A brief overview is provided for the

analytical and numerical models that are compared with the current method. This is followed by an investigation of the quasi-static properties and anisotropy degree of the polycrystals. Finally, the numerical results for the attenuation and phase velocity of the polycrystals for low and intermediate frequencies are presented.

A classical approach to study polycrystalline materials is to replace the micro-inhomogeneous elastic polycrystal with a continuous random medium described by a local elastic stiffness tensor $C_{ijkl}(\mathbf{r}) = c_{ijkl} + \delta_{ijkl}(\mathbf{r})$ with mean isotropic stiffness c_{ijkl} and random fluctuation $\delta_{ijkl}(\mathbf{r})$. The mean elastic medium with tensor c_{ijkl} is called the reference medium and for a single-phase polycrystalline is considered to be the Voigt average. The fluctuations with respect to the mean elastic tensor $\delta_{ijkl}(\mathbf{r})$ are considered to be small and described by a two-point correlation function (TPC), giving the probability of two points lying in the same grain. Such a definition of the TPC function describes the fluctuation of the elastic stiffness and the geometrical properties of the crystals. Given such a definition of the medium, the elastodynamic equations that govern polycrystalline materials constitute a system of partial differential equations with random coefficients. This is addressed either by the perturbative Keller approximation as used by Stanke and Kino [1], or equivalently by the first-order smoothing (Bourret) approximation of the Dyson equation as used by Weaver [36]. This approach is generally called SOA (Second Order Approximation) and is accurate when the crystals are not strongly anisotropic and the fluctuations with respect to the mean elastic tensor is small. To modify the SOA method for strongly anisotropic materials, Huang et al. [15] define a scattering parameter equivalent to the degree of inhomogeneity as an anisotropy index to categorize anisotropic materials and propose the direct approximation method (DAM) using this scattering parameter. In the DAM method, the phase velocity and attenuation in the Rayleigh limit are defined as a quadratic function of the scattering parameter and the quasi-static phase velocity of each polycrystal is modified based on its static properties evaluated by the self-consistent method [35]. This modification improved the estimation of the effective phase velocity for strongly anisotropic materials, however, the attenuation estimation remains inaccurate [15].

To compare the present method with other analytical and numerical methods, the results are compared with the calculations presented by Huang et al. [15]. As in the analytical methods, single phase polycrystals with randomly oriented crystallographic axes are considered in FEM [17]. The methodology of FEM including grain geometry, finite element spatial discretization, loading, and boundary conditions are described in detail by Van Pamel et al. [17]. The FEM results are of course not exact, both because of modeling issues (size of sample, generation of grains) and numerical issues (discretization errors, etc.). Specifically, for low frequency calculations, due to a change of mesh in the FE calculations [18], the inaccuracies in the FEM results are expected to be at least of the order of 5% [29].

The FE results compared in this study are based on multiple realizations with regard to the orientation of the crystals [15]. The geometrical model consists of 11,520 grains with a mean grain volume of $0.125\ \text{mm}^3$ and a variance of $0.0558\ \text{mm}^3$. Further discussion regarding the generation of the geometrical model, multiple realizations, and the effect of various grain size distributions can be found in the literature [16,17,37]. The analytical methods considered here have different considerations for the crystallography of the polycrystals and it is necessary to have a suitable correspondence of the geometrical models in the analytical methods and the one developed in the FE model. The geometrical properties required for the SOA and DAM models is the TPC function which describes the probability of two points in the medium lying in the same grain. An appropriate TPC function, according to the geometrical model generated by Van Pamel et al. [16] for the FE calculations, is determined by dropping two random points within the medium and through repetition calculate their probability of lying within a single grain [17]. The TPC function is then defined by an analytical fit to this measured distribution [6,17]. This TPC function is utilized in a comprehensive study by Huang et al. [15], and their results for SOA, DAM and FE methods are considered here for comparison with the SSA methods.

On the other hand, in the present method all crystals are assumed to be spheres with the same radius a. However, it is well established that the attenuation is significantly dependent on the actual grains sizes, and an accurate comparison of the present method requires consideration of statistical information regarding the grain size distribution. To compare the SSA methods, which assume a single grain size, with the SOA and DAM methods, which incorporate a grain size distribution, the volume of a single grain in the present method ($V = 4\pi a^3/3$) is set to be equal to the effective volume of the model used in both the SOA and DAM methods. The effective volume is defined by the volumetric integration of the TPC function, considering the fitted TPC function [6] to the FE model. The resulting effective grain volume is found to be $0.1459\ \text{mm}^3$, and the radius of the grains in the present model is adopted as $a = 0.3266\ \text{mm}$, which is used as the normalization radius in the subsequent calculations. It is worth noting that the effective grain volume ($0.1459\ \text{mm}^3$) is larger than the mean grain volume of the FE model ($0.125\ \text{mm}^3$).

Calculations for the present method are performed using Eqs. (51) and (50), first with the explicit expressions of the **T** matrix elements in the low frequency limit (which are referred to as the Rayleigh asymptote of the present methods (R-SSA-V and R-SSA-SC)), then with the numerical computations carried out with truncation at $l_{max} = m_{max} = 5$, and $j_{max} = 6$ (referred to as SSA-V and SSA-SC). For the calculations, Mathematica 12.3 is employed. The codes used to evaluate explicit expressions, as presented in the last section, are provided in the supplementary materials [38]. However, for the numerical evaluation of higher orders, the computational cost increases significantly. On a normal computer with a 3.2 GHz CPU and 64 GB RAM, the authors did not find it computationally reasonable to perform a calculation for higher orders. In general, to use the present approach for higher frequencies, it would be beneficial to analytically evaluate the parameters $H_{\tau\sigma ml}$ and $G_{\tau\sigma ml}$ (Eqs. (31) and (33)) for any orders. This is done for the simple case of scattering of SH waves by a transversely isotropic sphere [39].

At very low frequencies the attenuation tends to zero and the real effective wave numbers provide the static properties of the polycrystals. The quasi-static phase velocity of the polycrystalline materials in the DAM and SSA-SC methods are equal with the self-consistent method and it differs from the Voigt phase velocity as the anisotropy increases. The self-consistent method shows a good correspondence with FE and experimental evaluation [35] and is considered as accurate [15]. Table 2 presents macroscopic isotropic Lamé parameters for the 50 polycrystals examined in this study calculated using both Voigt and SC (static-consistent and self-consistent) averages. The measures of anisotropy degrees in the longitudinal (A_p) and transverse (A_s) directions are also presented in Table 2, together with the universal (A^U) [40] and log-Euclidean (A^L) [41] anisotropy indices. Fig. 2(a–b) displays the ratio of quasi-static effective phase velocity (C_i^{q-s}) to Voigt phase velocity (c_i) for (a) longitudinal (C_p^{q-s}/c_p) and (b) transverse (C_s^{q-s}/c_s) waves versus A_p and A_s, respectively. The quasi-static effective phase velocities are evaluated by SC (green dots), SSA-V (blue dots) and SOA (black dots) methods. The green dots show that the Voigt phase velocities have more than 5% difference with the accurate SC phase velocities when $A_i > 0.1$, and the error increases almost monotonically with respect to A_i for more anisotropic materials. It is also observed that the SSA-V quasi-static phase velocities has less than 1% difference with SC phase velocities when $A_i < 0.1$ and the difference increases monotonically to more than 5% for materials with $A_i > 0.2$. On the other hand, the SOA quasi-static phase velocities are accurate when $A_i < 0.05$ and do not show a clear monotonic relation with anisotropy degree. To compare the introduced measures of anisotropy degree with universal and log-Euclidean anisotropy indices, Fig. 2(c–d) displays the ratio of self-consistent effective phase velocity (C_i^{sc}) to Voigt phase velocity (c_i) for c) longitudinal (C_p^{sc}/c_p) and d) transverse (C_s^{sc}/c_s) waves, respectively, versus A^U (dark green dots) and A^L (red dots). The materials with extreme anisotropy indices are excluded from these figures for clarity. Comparing Fig. 2(c–d) with the green dots in Fig. 2(a–b) reveals that A_p and A_s

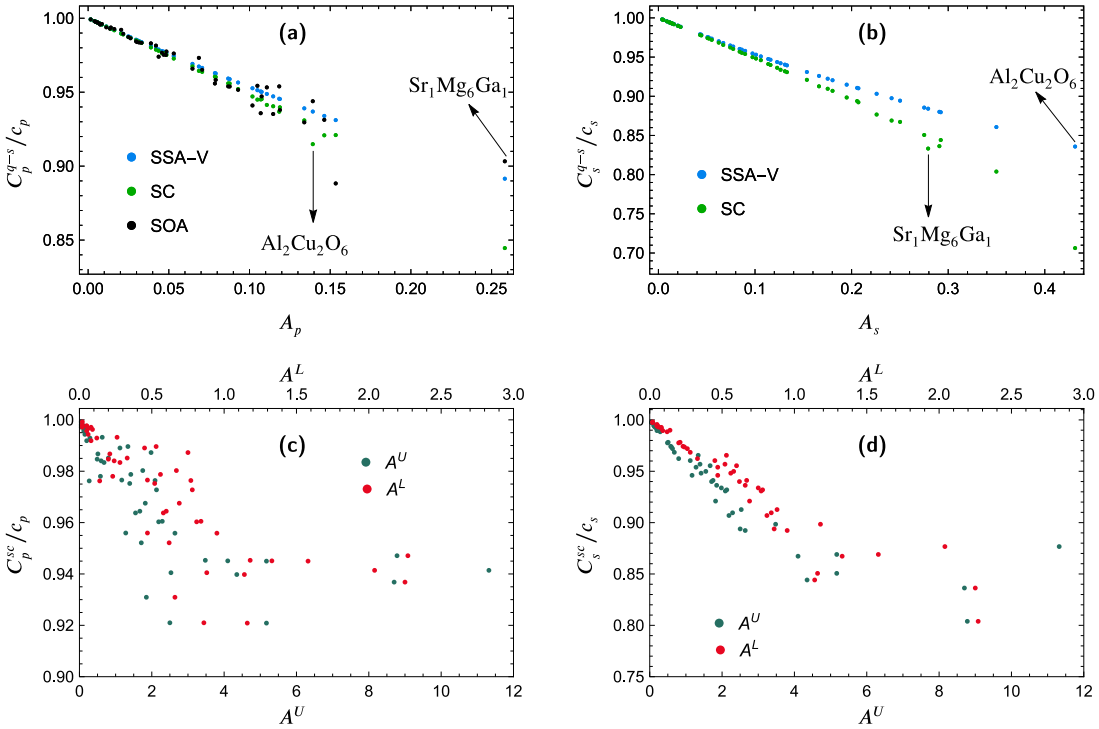

Fig. 2. The ratio of quasi-static phase velocities to Voigt phase velocities for (a) longitudinal (C_p^{q-s}/c_p) and (b) transverse (C_s^{q-s}/c_s) waves, versus longitudinal anisotropy degree A_p and transverse anisotropy degree A_s, respectively. Quasi-static phase velocities are evaluated by SSA-V (blue dots), SC (green dots), and SOA (Black dots) for 50 polycrystals of Table 2. The ratio of SC quasi-static phase velocities to Voigt phase velocities for longitudinal (C_p^{sc}/c_p) and transverse (C_s^{sc}/c_s) waves is depicted in Figure (c) and (d), respectively. The anisotropy indices A^U are shown on the bottom x-axis as dark green dots, while A^L is represented on the top x-axis as red dots.

have a better monotonic relation with accurate SC results compared to A^U and A^L. This is partly due to the separation of the degree of anisotropy in the longitudinal and transverse directions, whereas anisotropy indices aim to indicate the anisotropy of a material with a single parameter, disregarding the direction. However, as shown in Table 2 and Fig. 2(a–b), a material may have quite different degrees of anisotropy in various directions.

In the following, longitudinal attenuation and phase velocity for the materials listed in Table 2 are evaluated using the SSA, SOA, and DAM methods, with a focus on strongly anisotropic materials in the longitudinal direction.

The longitudinal attenuation and phase velocity are calculated for the materials listed in Tables 2 and 3, ordered based on the longitudinal anisotropy A_p for each symmetry of the crystals. Considering the good correspondence of the present methods for estimation of the attenuation and phase velocity for weakly anisotropic materials, the study is focused on strongly anisotropic materials. However, normalized root-mean-square deviation (NRMSD) of the longitudinal attenuation with respect to FEM is presented in Table 3 for all materials. NRMSD quantifies the overall difference in the frequency range of $k_p a \leq 0.5$ and is calculated as root mean square of $(\alpha_p^{\text{Model}}/\alpha_p^{\text{FEM}} - 1)$.

In the following the normalized longitudinal attenuation $\alpha_p a$ and normalized longitudinal phase velocity C_p/c_p are depicted versus normalized frequency $k_p a$ for different materials. The normalization parameters, c_p and k_p, are determined by the Voigt average. For each material, the quantities are calculated with the R-SSA-V method (dashed blue lines), SSA-V method (solid blue lines), R-SSA-SC method (dashed green lines), SSA-SC method (solid green lines), SOA method (dotted black lines), DAM method (solid red lines), and the FEM results (circles).

Fig. 3 shows (a) normalized longitudinal attenuation $\alpha_p a$ and (b) normalized longitudinal phase velocity C_p/c_p versus normalized frequency $k_p a$ for the strongest anisotropic materials in the longitudinal ($Sr_1Mg_6Ga_1$) and transverse ($Al_2Cu_2O_6$) cases. Fig. 4 shows normalized longitudinal attenuation $\alpha_p a$ versus normalized frequency $k_p a$ for the three polycrystals of, orthorhombic, tetragonal, hexagonal and cubic symmetries with the highest anisotropy factors A_p as stated in Table 2 (excluding the materials shown in Fig. 3). Finally, Fig. 5 shows normalized longitudinal phase velocity C_p/c_p versus normalized frequency $k_p a$ for the same polycrystals as in Fig. 4.

Combining the results of Figs. 3–5 and Table 2, the following observations are of interest:

The R-SSA-V and R-SSA-SC methods are valid only in the Rayleigh limit when the wavelength is much larger than the grain radius. In this frequency range they should be very attractive to use due to their simplicity and the fact that they are valid also for strong anisotropy. The range of validity of the Rayleigh results are somewhat hard to specify as it can vary significantly depending on the degree of anisotropy, ranging from $k_p a > 0.5$ for weakly anisotropic materials to $k_p a < 0.1$ for strongly anisotropic materials, such as $Sr_1Mg_6Ga_1$. The $Sr_1Mg_6Ga_1$ crystals possess orthorhombic symmetry, with different longitudinal wavenumbers along each coordinate axis. The ratio of these wavenumbers to the Voigt wave number of the macroscopically isotropic medium is $k_p^x/k_p = 0.82$, $k_p^y/k_p = 1.65$, and $k_p^z/k_p = 0.66$ for longitudinal wave numbers in the x, y, and z directions, respectively. The significant variation in wave velocities in different directions inside the crystals impacts the range of validity of the Rayleigh results.

For the phase velocity evaluation, the SSA-V method estimation of phase velocity shows a good correspondence with FEM for $A_p < 0.1$, however, the difference with FE calculation increases for higher degrees of anisotropy. On the other hand, for the DAM and SSA-SC methods all studied materials (except $Sr_1Mg_6Ga_1$) show good agreement with FEM results. Theoretically, DAM quasi-static phase velocity should be equal to R-SSA-SC phase velocity and the small differences that appear for the strongly anisotropic materials seem to be due to the fewer iterations considered in the evaluation of the self-consistent phase velocity by Huang et al. [15].

Table 3
NRMSD with respect to FEM in longitudinal attenuation for SOA, DAM, SSA-V, and SSA-SC methods [15].

Type	Material	A_p	α_p NRMSD to FEM (%)				Material	A_p	α_p NRMSD to FEM (%)			
			SOA	DAM	SSA-V	SSA-SC			SOA	DAM	SSA-V	SSA-SC
Orthorhombic	Co_2Se_4	4,6E−03	4,35	9,74	1,00	0,93	Enstatite	8,5E−03	25,40	17,51	4,14	2,61
	Ni_2SiO_4	1,1E−02	8,45	13,88	6,56	4,85	Fe_2SiO_3	1,6E−02	24,92	19,47	2,53	1,79
	Fe_2SiO_4	2,6E−02	5,17	3,37	6,76	1,92	U	3,0E−02	5,26	5,62	5,52	1,45
	Ca_2Ag_4	4,4E−02	40,43	35,41	5,11	1,42	Sn_4Pd_40	5,3E−02	36,38	5,50	12,65	1,75
	Mo_4O_{10}	8,7E−02	5,05	8,91	19,13	6,98	$Li_4Nb_4N_8$	9,3E−02	19,61	4,48	27,06	2,74
	$Na_2Cu_1O_2$	1,1E−01	4,64	37,11	24,40	8,01	$Na_2U_1O_4$	1,5E−01	65,13	55,74	33,95	13,49
	Te_8O_16	1,3E−01	14,23	4,84	30,30	11,52	$Sr_1Mg_6Ga_1$	2,6E−01	90,15	66,77	82,99	59,39
Tetragonal	Mg_1Al_3	4,9E−03	1,84	1,60	6,03	6,62	Sm_4O_2	5,7E−03	17,41	9,26	5,21	4,66
	Sn	2,0E−02	52,22	10,96	2,70	3,32	PDP	2,2E−02	20,07	5,26	4,44	2,42
	K_2N_6	3,2E−02	6,75	4,65	10,78	5,85	Zr_1H_2	4,6E−02	19,24	8,98	12,30	3,16
	Rutile	4,9E−02	32,78	3,71	14,77	4,63	NSH	7,1E−02	22,84	5,32	14,62	3,61
	RDP	1,1E−01	33,03	14,60	21,96	5,07	To	1,1E−01	61,90	20,14	33,04	6,97
	$Li_2C_1N_2$	1,1E−01	6,53	10,56	22,03	2,13	$Tl_2Cu_1F_4$	1,5E−01	46,38	7,33	41,02	12,02
Hexagonal	α − Be	3,9E−03	6,65	26,15	6,39	6,71	α − Ti	5,8E−03	1,46	1,63	5,05	5,41
	α − Co	7,5E−03	31,41	34,72	1,28	1,02	Nb_4N_4	1,4E−02	25,72	19,81	0,94	2,82
	α − Tl	2,5E−02	13,04	8,38	5,11	4,14	Mn_2Sb_2	3,3E−02	9,25	0,68	7,13	3,28
	Mn_2Bi_2	4,8E−02	7,93	2,18	3,33	3,15	Zn	6,9E−02	58,04	14,91	26,92	12,28
	Ba_2	7,9E−02	2,29	28,24	11,46	2,35	Be_2Se_2	1,0E−01	18,90	39,05	24,24	5,19
	Sr_4Si_2	1,0E−01	47,36	2,75	23,12	2,70	$Al_2Cu_2O_6$	1,4E−01	77,39	36,26	55,18	18,68
Cubic	Al	1,6E−03	8,43	1,63	1,66	1,74	Cr	6,8E−03	2,44	6,24	0,86	0,90
	Nb	1,4E−02	3,43	9,91	2,73	1,84	RbF	3,0E−02	1,85	13,33	6,90	4,71
	Cu	3,9E−02	36,62	7,74	8,91	2,67	In	4,2E−02	34,01	9,49	7,95	2,08
	As_1	4,7E−02	1,94	11,66	8,35	4,30	RbCl	6,5E−02	4,07	11,84	11,58	5,15
	RbBr	7,9E−02	5,34	11,19	13,34	5,53	RbI	8,8E−02	7,30	11,37	14,43	5,85
	Li	1,2E−01	63,91	9,79	34,10	7,37	Dy_1S_1	1,2E−01	14,70	12,37	19,85	7,11

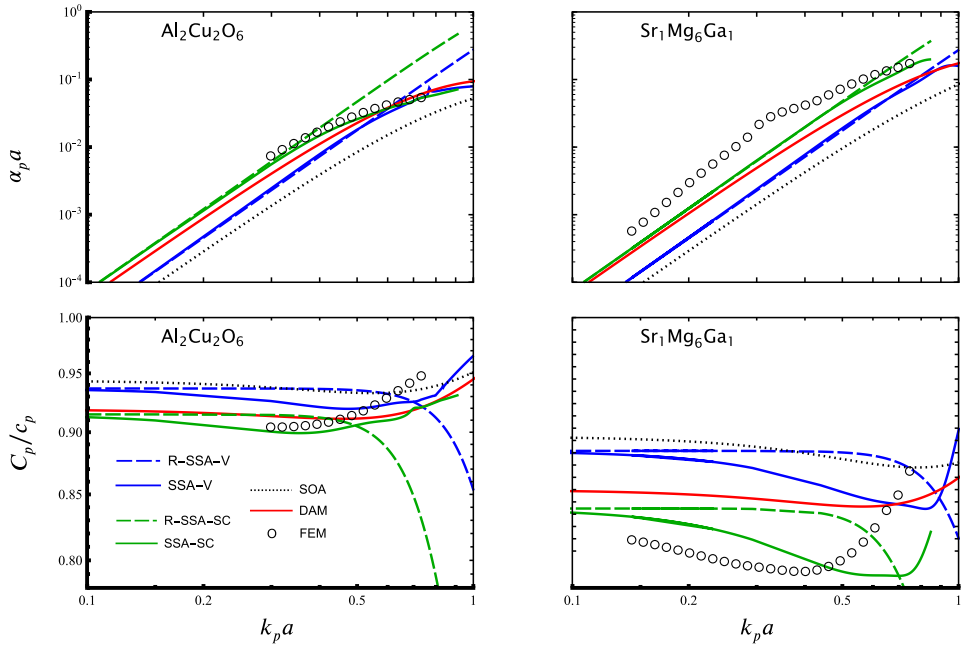

Fig. 3. Normalized attenuation $\alpha_p a$ and normalized phase velocity C_p/c_p versus normalized frequency $k_p a$ for longitudinal waves evaluated by the Rayleigh asymptote of the SSA methods, R-SSA-V (dashed blue lines), R-SSA-SC (dashed green lines), numerical evaluation of the SSA methods, SSA-V (solid blue lines), SSA-SC (solid green lines), SOA (dotted black lines), DAM method (solid red lines) and numerical FEM results (circles), for $Al_2Cu_2O_6$ and $Sr_1Mg_6Ga_1$ with highest transverse and longitudinal anisotropy degree, respectively.

For the attenuation estimation, the correspondence of the SSA methods with FEM results has an almost monotonic correlation with the anisotropy degree A_p. The SSA-V method shows a good agreement with NRSMD less than 10% for materials with $A_p < 0.1$, while the SSA-SC method shows such correspondence for all materials except $Sr_1Mg_6Ga_1$ with $A_p = 0.26$. On the other hand, the correspondence of SOA and DAM methods with FEM are not directly related to the anisotropy degree A_p. Overall, both methods show better correspondence with FEM for weakly anisotropic materials, and the agreement of DAM is higher than the SOA method. However, there are plenty of exceptions for all types of crystal symmetries. As the accuracy of the FEM results depend on several factors discussed in the last section, the validity of the mentioned analytical approaches is best to be examined with experimental results.

For $Sr_1Mg_6Ga_1$, with an extremely high degree of anisotropy, none of the studied methods has a good agreement with FEM. The lowest NRMSD in the range of $0.15 < k_p a < 0.5$ is for the SSA-SC method with 3% difference for the phase velocity and 60% difference for the attenuation.

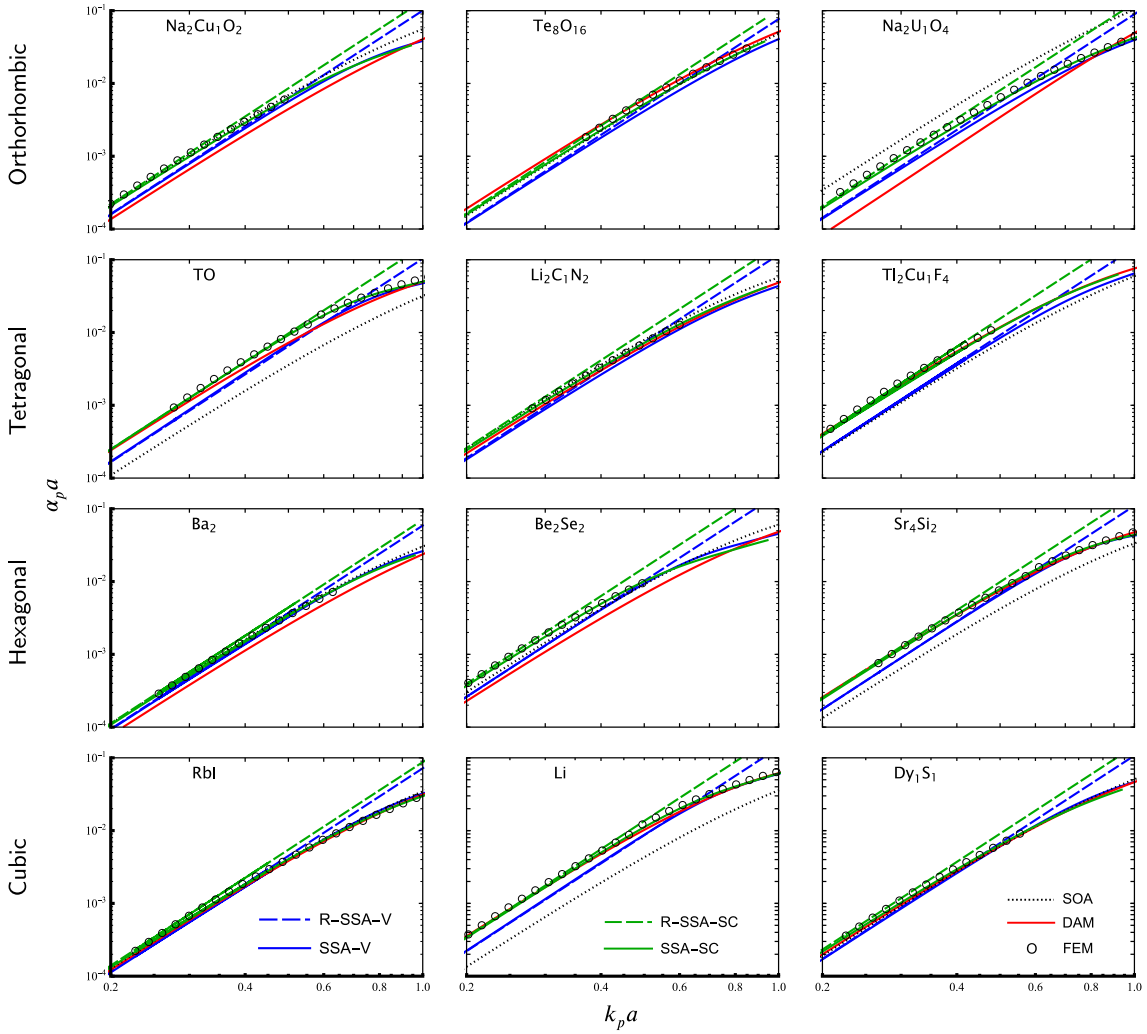

Fig. 4. Normalized attenuation $\alpha_p a$ versus normalized frequency $k_p a$ for longitudinal waves evaluated by the Rayleigh asymptote of the SSA methods, R-SSA-V (dashed blue lines), R-SSA-SC (dashed green lines), numerical evaluation of the SSA methods, SSA-V (solid blue lines), SSA-SC (solid green lines), DAM method (solid red lines), and numerical FEM results (circles), for three highly anisotropic polycrystals of cubic, hexagonal, tetragonal and orthorhombic symmetries.

This appears to be due to the high degree of anisotropy and strong attenuation, even at low frequencies. As a result, the frequency range of $0.15 < k_p a < 0.5$ is beyond the Rayleigh limit for this material and is in the region where the geometrical properties of crystals are becoming significant. This confirms that the Rayleigh limit not only depends on the ratio of the grain size and wavelength, but also on the elasticity of the grains and the attenuation.

7. Concluding remarks

This paper examines the scattering of elastic waves by an anisotropic sphere with orthorhombic symmetry in an isotropic environment. To accomplish this spherical coordinates are utilized and the displacement field inside the sphere is expanded in terms of vector spherical harmonics in the angular coordinates and powers in the radial coordinate. This leads to recursion relations among the expansion coefficients. The boundary conditions on the sphere are then used to determine the elements of the transition matrix (**T**). At low frequencies the leading order elements are expressed explicitly in simple form. The contributions of monopole, dipole, and quadrupole elements are all taken into account. The dipole elements are not coupled to the other elements and depend solely on the density of the sphere, and are, in fact, the same as for an isotropic sphere. The monopole elements, however, are coupled with the quadrupole elements for even waves of even order ($\sigma = e$ and $m = 0, 2$) in azimuthal coordinates. These elements depend on the elasticity of the sphere but not on the density or shear moduli. On the other hand, the remaining quadrupole elements are uncoupled and only depend on the shear moduli of the sphere.

Furthermore, the wave propagation in single phase polycrystalline materials with cubic, hexagonal, tetragonal, and orthorhombic symmetry of the crystals is analyzed using the Foldy theory. To assess the degree of anisotropy of the grains, two parameters for measuring degrees of anisotropy in longitudinal and transverse directions are introduced. The Voigt average has typically been used to calculate the unperturbed elasticity constants for determining attenuation and phase velocity in polycrystals. However, this method seems to be not suitable for highly anisotropic materials as it does not show a good agreement in quasi static phase velocity estimation with accurate SC results. To address this, a new methodology is proposed that calculates the average macroscopic homogenized and isotropic properties of polycrystals. This average is shown to be equivalent with self

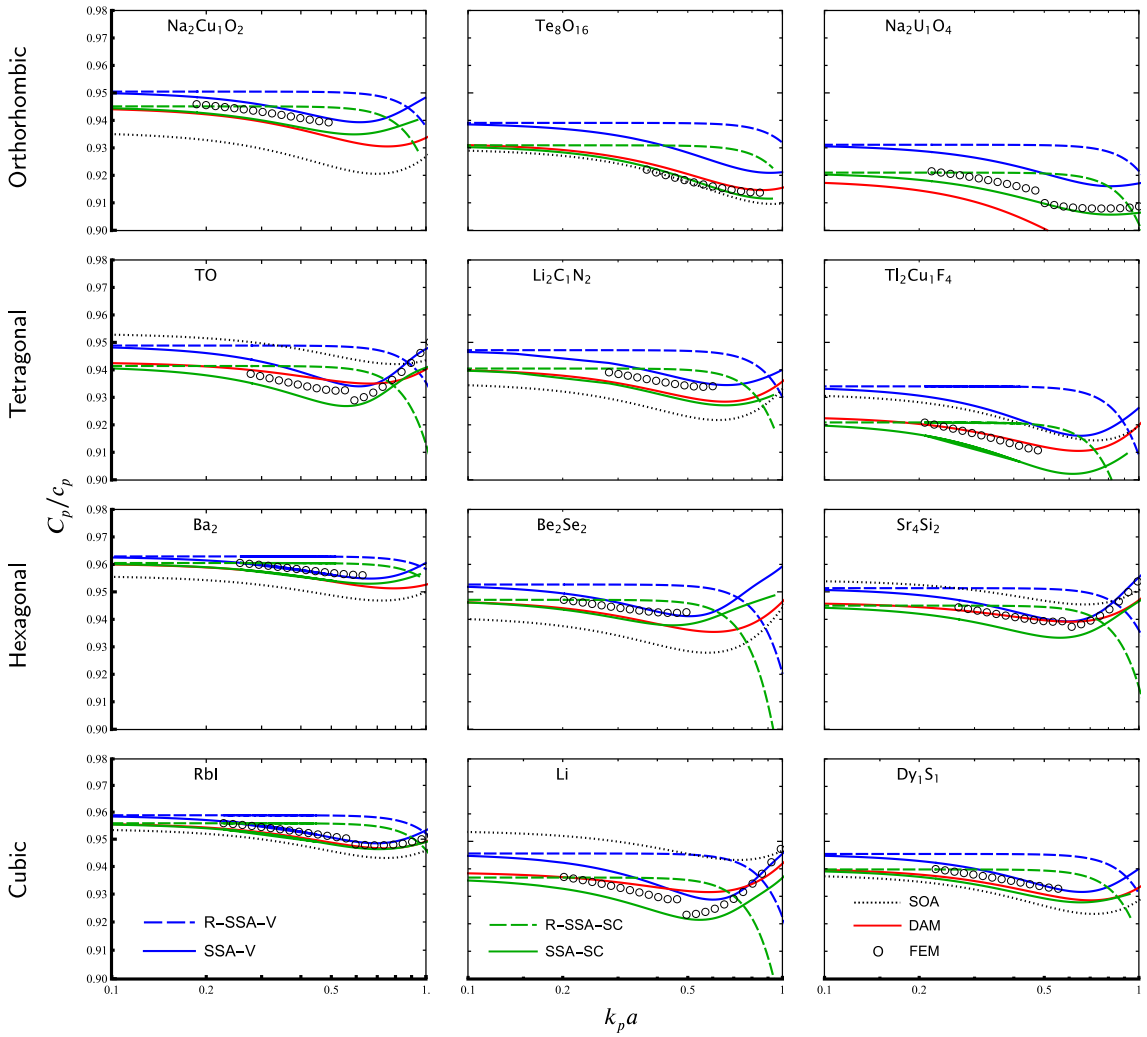

Fig. 5. Normalized phase velocity C_p/c_p versus normalized frequency k_pa for longitudinal waves evaluated by the Rayleigh asymptote of the SSA methods, R-SSA-V (dashed blue lines), R-SSA-SC (dashed green lines), numerical evaluation of the SSA methods, SSA-V (solid blue lines), SSA-SC (solid green lines), SOA (dotted black lines), DAM method (solid red lines), and numerical FEM results (circles), for three highly anisotropic polycrystals of cubic, hexagonal, tetragonal and orthorhombic symmetries. The SOA method for $Na_2U_1O_4$ yields a phase velocity that is outside the current plotting range.

consistent average. Furthermore, adopting this average for the properties of the matrix exhibit better agreement with FE results for calculations of attenuation and phase velocity.

The present method is compared to other theories and numerical FEM computations from the literature, and the results exhibit very good agreement with FEM for low frequencies and high anisotropy. Specifically, when comparing the SOA with SSA-V and DAM with SSA-SC methods, the present method demonstrates significant advantages for evaluating the attenuation in strongly anisotropic polycrystalline materials in the low and medium frequency ranges. However, it should be noted that other methods do not have the frequency limitation of the present method.

The present method is restricted to low frequencies due to various factors. The explicit form of the **T** matrix elements utilized in the method is only reliable for low frequencies. Although a numerical computation of additional **T** matrix elements can extend the frequency range, this approach is more computationally complex. The use of the Foldy theory is another limitation, which could potentially be addressed by incorporating more refined multiple scattering theories. Furthermore, the present approach assumes spherical grains, which is appropriate for low frequencies where the scattering is mainly a volume effect, but may be inadequate at higher frequencies.

The present methods can be expanded and improved in various ways. In the current approach only spheres of the same size are considered. However, within the Foldy theory framework it is feasible to explore a distribution of sphere sizes, which would provide a more realistic representation of many polycrystalline materials. Additionally, the present method can be extended to study particulate composite materials with multiple phases, which would offer a broader scope for potential applications. These potential improvements and extensions to the present method offer interesting opportunities to advance the understanding of wave propagation in composite materials.

Declaration of competing interest

The authors declare the following financial interests/personal relationships which may be considered as potential competing interests: Anders Boström reports financial support was provided by Swedish Research Council. Anders Boström reports a relationship with Swedish Research Council that includes: funding grants.

Data availability

I have shared the link to my code in the attached file

Supplementary Documents (Original data) (Figshare)

Acknowledgments

The FE, SOA and DAM results that are used as a comparison have very kindly been provided by Prof. M. Lowe and Dr. M. Huang, Imperial College, London.

The present project is funded by the Swedish Research Council [grant number 2017-03958] and this is gratefully acknowledged.

References

[1] F.E. Stanke, G.S. Kino, A unified theory for elastic wave propagation in polycrystalline materials, J. Acoust. Soc. Am. 75 (3) (1984) 665–681, http://dx.doi.org/10.1121/1.390577.
[2] X. Bai, B. Tie, J.-H. Schmitt, D. Aubry, Comparison of ultrasonic attenuation within two- and three-dimensional polycrystalline media, Ultrasonics (ISSN: 0041-624X) 100 (2020) 105980, http://dx.doi.org/10.1016/j.ultras.2019.105980.
[3] L. Yang, O.I. Lobkis, S.I. Rokhlin, Shape effect of elongated grains on ultrasonic attenuation in polycrystalline materials, Ultrasonics 51 (6) (2011) 697–708, http://dx.doi.org/10.1016/j.ultras.2011.02.002.
[4] O.I. Lobkis, L. Yang, J. Li, S.I. Rokhlin, Ultrasonic backscattering in polycrystals with elongated single phase and duplex microstructures, Ultrasonics 52 (6) (2012) 694–705, http://dx.doi.org/10.1016/j.ultras.2011.12.002.
[5] J. Li, L. Yang, S.I. Rokhlin, Effect of texture and grain shape on ultrasonic backscattering in polycrystals, Ultrasonics 54 (7) (2014) 1789–1803, http://dx.doi.org/10.1016/j.ultras.2014.02.020.
[6] G. Sha, M. Huang, M.J.S. Lowe, S.I. Rokhlin, Attenuation and velocity of elastic waves in polycrystals with generally anisotropic grains: Analytic and numerical modeling, J. Acoust. Soc. Am. 147 (4) (2020) 2442–2465, http://dx.doi.org/10.1121/10.0001087.
[7] M. Norouzian, S. Islam, J.A. Turner, Influence of microstructural grain-size distribution on ultrasonic scattering, Ultrasonics (ISSN: 0041-624X) 102 (2020) 106032, http://dx.doi.org/10.1016/j.ultras.2019.106032.
[8] L. Yang, O.I. Lobkis, S.I. Rokhlin, Explicit model for ultrasonic attenuation in equiaxial hexagonal polycrystalline materials, Ultrasonics 51 (3) (2011) 303–309, http://dx.doi.org/10.1016/j.ultras.2010.10.002.
[9] L. Yang, J. Li, S.I. Rokhlin, Ultrasonic scattering in polycrystals with orientation clusters of orthorhombic crystallites, Wave Motion 50 (8) (2013) 1283–1302, http://dx.doi.org/10.1016/j.wavemoti.2013.06.003.
[10] C.M. Kube, J.A. Turner, Acoustic attenuation coefficients for polycrystalline materials containing crystallites of any symmetry class, J. Acoust. Soc. Am. 137 (6) (2015) 476–482, http://dx.doi.org/10.1121/1.4921676.
[11] S. Rokhlin, G. Sha, J. Li, A. Pilchak, Inversion methodology for ultrasonic characterization of polycrystals with clusters of preferentially oriented grains, Ultrasonics (ISSN: 0041-624X) 115 (2021) 106433, http://dx.doi.org/10.1016/j.ultras.2021.106433.
[12] A. Renaud, B. Tie, A.-S. Mouronval, J.-H. Schmitt, Multi-parameter optimization of attenuation data for characterizing grain size distributions and application to bimodal microstructures, Ultrasonics (ISSN: 0041-624X) 115 (2021) 106425, http://dx.doi.org/10.1016/j.ultras.2021.106425.
[13] C.M. Kube, J.A. Turner, Ultrasonic attenuation in polycrystals using a self-consistent approach, Wave Motion (ISSN: 0165-2125) 57 (2015) 182–193, http://dx.doi.org/10.1016/j.wavemoti.2015.04.002.
[14] A. Van Pamel, G. Sha, M.J.S. Lowe, S.I. Rokhlin, Numerical and analytic modelling of elastodynamic scattering within polycrystalline materials, J. Acoust. Soc. Am. 143 (4) (2018) 2394–2408, http://dx.doi.org/10.1121/1.5031008.
[15] M. Huang, S.I. Rokhlin, M.J.S. Lowe, Appraising scattering theories for polycrystals of any symmetry using finite elements, Trans. R. Soc. A 380 (2231) (2022) 20210382, http://dx.doi.org/10.1098/rsta.2021.0382.
[16] A. Van Pamel, C.R. Brett, P. Huthwaite, M.J.S. Lowe, Finite element modelling of elastic wave scattering within a polycrystalline material in two and three dimensions, J. Acoust. Soc. Am. 138 (4) (2015) 2326–2336, http://dx.doi.org/10.1121/1.4931445.
[17] A. Van Pamel, G. Sha, S.I. Rokhlin, M.J.S. Lowe, Finite-element modelling of elastic wave propagation and scattering within heterogeneous media, Proc. R. Soc. Lond. Ser. A Math. Phys. Eng. Sci. 473 (2197) (2017) 20160738, http://dx.doi.org/10.1098/rspa.2016.0738.
[18] M. Huang, G. Sha, P. Huthwaite, S.I. Rokhlin, M.J.S. Lowe, Maximizing the accuracy of finite element simulation of elastic wave propagation in polycrystals, J. Acoust. Soc. Am. 148 (4) (2020) 1890–1910, http://dx.doi.org/10.1121/10.0002102.
[19] M. Huang, P. Huthwaite, S.I. Rokhlin, M.J.S. Lowe, Finite-element and semi-analytical study of elastic wave propagation in strongly scattering polycrystals, Proc. R. Soc. Lond. Ser. A Math. Phys. Eng. Sci. 478 (2258) (2022) 20210850, http://dx.doi.org/10.1098/rspa.2021.0850.
[20] Y. Huang, J.A. Turner, Y. Song, X. Li, Transverse-to-transverse diffuse ultrasonic double scattering, Ultrasonics (ISSN: 0041-624X) 111 (2021) 106301, http://dx.doi.org/10.1016/j.ultras.2020.106301.
[21] L.L. Foldy, The multiple scattering of waves. I. General theory of isotropic scattering by randomly distributed scatterers, Phys. Rev. 67 (3–4) (1945) 107–119, http://dx.doi.org/10.1103/PhysRev.67.107.
[22] M. Lax, Multiple scattering of waves. II. The effective field in dense systems, Phys. Rev. 85 (4) (1952) 621, http://dx.doi.org/10.1103/PhysRev.85.621.
[23] A.K. Mal, L. Knopoff, Elastic wave velocities in two-component systems, IMA J. Appl. Math. 3 (4) (1967) 376–387, http://dx.doi.org/10.1093/imamat/3.4.376.
[24] J.E. Gubernatis, E. Domany, Effects of microstructure on the speed and attenuation of elastic waves in porous materials, Wave Motion 6 (6) (1984) 579–589, http://dx.doi.org/10.1016/0165-2125(84)90048-9.
[25] S. Kanaun, V. Levin, Self-Consistent Methods for Composites: Vol. 2: Wave Propagation in Heterogeneous Materials, Springer Science & Business Media, 2009.
[26] A. Boström, Scattering by an anisotropic circle, Wave Motion 57 (2015) 239–244, http://dx.doi.org/10.1016/j.wavemoti.2015.04.007.
[27] A. Boström, Scattering of in-plane elastic waves by an anisotropic circle, Q. J. Mech. Appl. Math. 71 (2018) 139–155, http://dx.doi.org/10.1093/qjmam/hbx029.
[28] A. Jafarzadeh, P.D. Folkow, A. Boström, Scattering of elastic waves by a transversely isotropic sphere and ultrasonic attenuation in hexagonal polycrystalline materials, Wave Motion (ISSN: 0165-2125) 112 (2022) 102963, http://dx.doi.org/10.1016/j.wavemoti.2022.102963.
[29] A. Jafarzadeh, P.D. Folkow, A. Boström, Scattering of elastic waves by a sphere with cubic anisotropy with application to attenuation in polycrystalline materials, Proc. R. Soc. Lond. Ser. A Math. Phys. Eng. Sci. 479 (2272) (2023) 20220476, http://dx.doi.org/10.1098/rspa.2022.0476.
[30] V.V. Varadan, A. Lakhtakia, V.K. Varadan, Field Representations and Introduction To Scattering, North-Holland, Amsterdam, 1991.
[31] A. Boström, Scattering by a smooth elastic obstacle, J. Acoust. Soc. Am. 67 (6) (1980) 1904–1913, http://dx.doi.org/10.1121/1.384455.
[32] P.C. Waterman, Matrix theory of elastic wave scattering, J. Acoust. Soc. Am. 60 (3) (1976) 567–580, http://dx.doi.org/10.1121/1.381130.
[33] J.B. Keller, Stochastic equations and wave propagation in random media, in: R. Bellman (Ed.), Proceedings of Symposia in Applied Mathematics Stochastic Processes in Mathematical Physics and Engineering, Providence, RI: American Mathematical Society, 2020, pp. 145–179.
[34] R. Bourret, Stochastically perturbed fields, with applications to wave propagation in random media, Nuovo Cimento 26 (1962) 1–31, http://dx.doi.org/10.1007/BF02754339.
[35] C.M. Kube, M. De Jong, Elastic constants of polycrystals with generally anisotropic crystals, J. Appl. Phys. 120 (16) (2016) 165105, http://dx.doi.org/10.1063/1.4965867.
[36] R.L. Weaver, Diffusivity of ultrasound in polycrystals, J. Mech. Phys. Solids 38 (1) (1990) 55–86, http://dx.doi.org/10.1016/0022-5096(90)90021-U.
[37] M. Ryzy, T. Grabec, P. Sedlák, I.A. Veres, Influence of grain morphology on ultrasonic wave attenuation in polycrystalline media with statistically equiaxed grains, J. Acoust. Soc. Am. 143 (1) (2018) 219–229, http://dx.doi.org/10.1121/1.5020785.

[38] A. Jafarzadeh, P.D. Folkow, A. Boström, Scattering of elastic waves by a sphere with orthorhombic anisotropy and application to polycrystalline material characterization-supplementary documents, 2023, http://dx.doi.org/10.6084/m9.figshare.23878839.
[39] A. Jafarzadeh, P.D. Folkow, A. Boström, Scattering of elastic SH waves by transversely isotropic sphere, in: Proceedings of the International Conference on Structural Dynamic , EURODYN, vol. 2, 2020, pp. 2782–2797, http://dx.doi.org/10.47964/1120.9228.18744.
[40] S.I. Ranganathan, M. Ostoja-Starzewski, Universal elastic anisotropy index, Phys. Rev. Lett. 101 (2008) 055504, https://link.aps.org/doi/10.1103/PhysRevLett.101.055504.
[41] C.M. Kube, Elastic anisotropy of crystals, AIP Adv. 6 (9) (2016) 095209, http://dx.doi.org/10.1063/1.4962996.